UTRECHT UNIVERSITY

Applying Artificial Neural Networks to Predict Effects of Microbial Degradation on Physical Reservoir Parameters in Geothermal and Carbon Capture and Storage Settings

by

A. van Veen

October 2018

UTRECHT UNIVERSITY

Abstract

Geoscience

Master of Science

by A. van Veen

In this research, the influence of microbial degradation on the porosity and permeability of sedimentary reservoirs is explored. Bentheimer Sandstone samples are exposed to a a total of nine different metabolite concentration and temperature conditions. Relative impact of initial porosity and permeability values and temperature and concentration conditions on changes in porosity and permeability are explored using an artificial neural network. Predictive ability of the neural network is limited but performance should improve with increased sample size and addition of more input parameters. Liquid permeability of Bentheimer sandstone decreases up to 40 percent. Both dry and liquid porosity decrease up to 10 percent. In situ mobilisation of fines could be a mechanism that explains decrease in effective permeability and porosity. Further insight into the physical and chemical processes that govern porosity and permeability change could be gained by expanding the research to include more controlled parameters and increase sample sizes.

Acknowledgements

I thank Caroline Lievens and Kathrin Zweers for the support in the lab at ITC and Robert Hack for general guidance and writing revision. Thanks goes out to Marco Madirisha for input on microbiology.

I am indebted to the technical team at the rock mechanics lab at the TU Delft, in particular Wim Verwaal, for support in sample preparation and measurements. I am also indebted to Leonard Bik and Hans de Bresser at Utrecht University for support in creating thin sections. I thank Amir Raoof for writing revision.

I am thankful for all the support my parents gave me, without whom I could not have done this.

I thank Karina for building memories with me in Enschede and for teaching me in all things outside of science.

I thank the PhD's and interns at ITC-ESA for becoming friends with interesting perspectives.

Contents

List of Figures

List of Tables

Abbreviations

CCS	**C**arbon **C**apture and **S**equestration
L-BFGS Solver	**L**imited Memory **B**royden-**F**letcher-**G**oldfarb-**S**hanno Solver
MLP	**M**ulti **L**ayer **P**erceptron
SRB	**S**ulphur **R**educing **B**acteria
SRP	**S**ulphur **R**educing **P**rokaryote

Wet p	Refers to effective porosity for liquids
Wet perm	Refers to effective permeability for liquids
Dry p	Refers to effective porosity for gases
Dry perm	Refers to effective permeability for gases

Physical Constants

MOLECULAR WEIGHTS		
Acetic Acid	60.05	(g/mol)
Isobutyric Acid	88.11	(g/mol)
Isovaleric Acid	102.13	(g/mol)

Symbols

A	surface area	m^2
L	height	m
P	pressure gradient	Pa
K	permeability	D (Darcy)
V	volume	m^3
t	time	s
p	porosity	(-)
μ	viscosity	Nm

Chapter 1

Introduction

1.1 Geothermal energy production in sedimentary basins

Geothermal power plants harness the heat from the center of the Earth. Temperature increases with depth along the geotherm. Often, locations are chosen where there is a steep geotherm, such as volcanic areas and rift valleys as this results in higher temperatures closer to the surface. Still, in areas with an average geotherm incline, geothermal energy can be viable in deep sedimentary systems. Deep geothermal systems are geologically similar in nature to oil and gas fields. As an oil or gas field matures, it commonly sees an increased cut of water in produced fluids, in some cases up to 99 percent of the total production (Singh et al. [2017]). Water produced from oil or gas fields often has a temperature of 65-150C Liu et al. [2018]. In light the energy transition, research has been done on the viability of utilizing mature oil and gas fields as a geothermal source (e.g.: Barbacki [2000], Liu et al. [2018], Singh et al. [2017]). One of the major benefits of alternative utilization of mature oil and gas fields is the reduced capital expenditure of a geothermal project. Other than the conversion of old oil and gas sites, geothermal energy can be harnessed in deep sedimentary systems.

1.2 Use of carbon and capture and storage

With the production of geothermal fluids, some gases are produced as well. An important component of these gases is CO_2. For clean geothermal energy production, it could be

considered to reinject the CO2 into the reservoir, following a carbon and capture and sequestration procedure (CCS). CCS has been more widely considered as a technology that could aid reduction of atmospheric CO_2. Depleted oil and gas reservoirs and deep saline aquifers are common storage targets for CCS purposes.

1.3 The problem and previous research

The fluid production at any geothermal, oil, or gas field is highly dependent on the porosity and permeability of the reservoir rock. Many factors can influence permeability and porosity of a reservoir during production and/or injection and the topic has been widely researched. In the example of CCS, research has been performed on the effects of CO_2 and brines on porosity and permeability of reservoirs by Fischer et al. [2011]. Formation impairment in the setting of fluid reinjection has been studied among others by Ungemach [2003]. Ungemach mentions suspended solids such as corrosion products and scales as well as trapped gases among factors that can restrain flow through a reservoir close to an injection well head due to pore clogging. Dissolution of reservoir rock and precipitation of new minerals can also impact porosity and permeability of a reservoir. Finally, another mechanism that can impact physical properties of a reservoir rock is microbial degradation. Microbial influence on permeability and porosity of a rock can be subdivided into several factors. The physical presence of microbes could cause pore clogging which restricts the flow of fluids through the reservoir. Growth and decay of microbes can lead to sedimentation of microbes in intergranular pore space. To quantify the extent to which these factors impact porosity and permeability, it is needed to understand the transportation of microbes within porous media. Additionally, microbes can have an impact through the excretion of metabolites. In geothermal reservoirs as well as oil and gas reservoirs, thermophile microbes might be present. Within the oil and gas industry, the dangers of Sulphur Reducing Prokaryotes (SRPs) and more specifically Sulphur Reducing Bacteria (SRBs) are well known. SRBs tendency to excrete H_2S when in the presence of $C0_2$ can impact the quality of petroleum products and corrode pipelines. Similarly, other metabolites excreted by a range of microbes can corrode the reservoir rock. It should be noted that SRPs are often accompanied by other microbes, which can produce acids that can influence chemical equilibria and potentially accelerate corrosion. Especially secondary and tertiary chemical reactions

that can occur due to the combined presence of metabolites within a brine are poorly understood. Compared to studies towards oil and gas applications, research towards geothermal energy development is young and limited. Given the increase in geothermal exploitation globally, research on flow through sedimentary rock outside of typical oil and gas applications has an increased mandate. For CCS applications, permeability and porosity are important factors for storage capacity and injection rates of CO_2. Research on microbial influence on sedimentary reservoir rock in geothermal and CCS settings could improve understanding of opportunities and challenges in developing geothermal resources in sedimentary reservoirs as well as the development of CCS solutions.

1.4 Introduction of the collaboration

This research forms the MSc Thesis of A. van Veen BSc towards his degree in Earth, Structure and Dynamics at Utrecht University. The research has been performed at ITC-UTwente. Supervision at ITC-UTwente has been done by dr. R. Hack and dr. C. Lievens whereas Utrecht University oversight has been done by dr. A. Raoof. Data produced during the research are simultaneously aimed to reinforce the PhD of M. Madirisha. The effects of microbial reservoir degradation in the context of geothermal energy production, the transformation of mature oil and gas fields into geothermal energy sources and carbon capture and sequestration are covered as a part of the Nuffic Tanzania Dutch Energy Capacity Building (TDECB) Project [1]. The research aims to quantify microbial degradation of sandstone and to model these in a neural network to find an physical-mechanical biological relationship between initial rock properties, in-situ conditions, and physical properties of microbially degraded rock.

1.5 Context of research methodology

Laboratory experiments with a range of microbial products in sandstone in environments that represent geothermal fields and carbon injection settings could yield insight into the end member products of microbially deteriorated reservoir rock.

[1] Partners: The University of Twente, Hanze University of Applied Sciences in Groningen, Delft University of Technology, Utrecht University, the University of Dar es Salaam (UDSM), the Dar es Salaam Institute of Technology (DIT),Karume Institute of Science and Technology (KIST) in Zanzibar

Reactive transport modelling that accurately describes the spreading of microbes through a reservoir as well as the chemical equilibria that accompany the presence of microbes is complex and requires the consideration of a high number of variables . Historically, models have therefore either focused on flow in a reservoir and have considered microbes as round particles that spread through advection, dispersion, and diffusion whereas other models have focused on the spreading of microbes through growth, decay, and sorption while assuming a static reservoir . The second method allows the incorporation of chemical processes into the model as well as the expected effects of biofilm formation Murphy and Ginn [2000]. Attempts to combine these processes in a single model have been done by among others Tufenkji (2007) and Murphy and Ginn (2000) but many questions still remain. In this research, an attempt is made to isolate the chemical effects of metabolites from thermophile microbes in a static regime and relate the effects on porosity and permeability to the initial properties of the reservoir rock and in-situ conditions. This still leaves a significant number of parameters that influence the end member products. The data generated by the laboratory experiment can be utilized as a training data set for a neural network to find a best fit and could allow the model to be used as a predictive tool for the evaluation of porosity and permeability in a sedimentary reservoir that might be impacted by the presence of microbes. This approach skips the complicated nature of the processes and explores the possibility of finding a simple way to predict the impact of microbial reservoir degradation in terms of porosity and permeability. To reach this goal, a neural network can be created that uses a machine learning algorithm and a data set provided by laboratory experiments. A Neural Network increases in accuracy with growing sample sizes. It is expected that sample size is insufficient for high accuracy predictions. Measurements from the PhD research following this thesis could improve performance of the network. A multi-layer perceptron assigns weights to input parameters in iterations while minimizing a loss function. The use of a multi-layer perceptron could yield insight into the relative impact of input parameters on the change of porosity and permeability in a sample.

Chapter 2

Methodology

The methods of this research can be subdivided into laboratory experiments and neural network implementation. The laboratory part consists of sample preparation, initial porosity and permeability recording, metabolite treatment, and final porosity and permeability recording. Each part is developed below.

2.1 Laboratory experiment

2.1.1 Sample preparation

Bentheimer Sandstone is selected to be used in the laboratory experiments. The Bentheimer Sandstone is a shallow marine deposit from the Early Cretaceous. It is well known as a petroleum reservoir rock and widely used as a building material Dubelaar and Nijland [2015]. The Bentheimer Sandstone ranges in permeability between 1.5-3.0 Darcy and has an average porosity of 0.248. Composition is over 90 % quartz, with minor occurrence of feldspar, clay minerals and iron oxides Peksa et al. [2015]. More detailed descriptions of the Bentheimer Sandstone can be found in Dubelaar and Nijland [2015] Peksa et al. [2015]. Bentheimer Sandstone has strong lateral continuity and homogeneity, which allows for the assumption that samples extracted from a block of Bentheimer Sandstone should have the same mineral content, porosity, and permeability. This makes Bentheimer Sandstone suitable for laboratory experiments Peksa et al. [2015]. Furthermore, sedimentary rock is relevant for a research on microbial degradation

since thermophile prokaryotes survive up to temperatures of 130 Celsius. Geothermal reservoirs with such temperatures are often of sedimentary nature rather than volcanic. Additionally, most oil and gas fields that may be converted into geothermal sites are of sedimentary origin.

Due to the deposition process and subsequent non-random alignment of grains, a sedimentary rock may show variable permeability in different directions, called anisotropy. Samples have been drilled along three perpendicular axes to create a limited range of permeabilities in the sample set in line with the anisotropy of the source rock. Cores have been taken in two perpendicular directions along the bedding plane (x and y-directions) and one perpendicular to the bedding plane (z-direction). 36 cylindric samples are taken with a diameter of 30mm and a height of 35mm. Additionally, large samples of 40mm diameter and 80mm height are taken for peak strength testing.

2.1.2 Initial state

The initial state of all samples is recorded with respect to dry porosity, dry permeability, wet porosity, and wet permeability. The values measured before treatment with metabolites will provide the base level from which changes in porosity and permeability can be quantified.

2.1.2.1 Dry Porosity

Measurements on dry porosity are done using the UltraPycnometer 1000. All samples have been run 8 times and an average porosity is taken for each sample. The Ultrapycnometer 1000 determines the true volume of a solid through by filling a compartment of known size with Helium gas and using Archimedes' principle of fluid displacement and the gas expansion law.

2.1.2.2 Dry Permeability

Dry permeability is measured using a Ruska gas permeameter. Due to high permeability of Bentheimer Sandstone, measurements were taken at pressure gradients of 0.05, 0.10

and 0.15 for all samples. The dry permeability is calculated following Darcy's law as shown in equation 2.1.

$$K = \frac{\mu Q L}{A P} \tag{2.1}$$

in which K is the permeability, μ is the viscosity of the gas, Q is the average flow rate of the gas, L is the height of the sample, A is the cross-sectional area of the sample and P is the pressure gradient along the sample.

2.1.2.3 Wet Porosity

Measurements on liquid porosity are done by first measuring the dry weight of the sample. Then follows immersion of the samples in Milli Q water [1] in a vacuum where after weighing the samples in submersion. Archimedes law is used to calculate the pore volume of each sample.

2.1.2.4 Wet Permeability

Wet permeability is measured with a Ruska liquid permeameter. The sample is pressed into a tight fitting rubber casing and water is pressed through the sample at a pressure gradient of 0.25 atmosphere. The amount of time it takes for 50 milliliters of water to pass through the sample is recorded. Finally, the liquid permeability can be calculated following Darcy's law as shown in equation 2.2.

$$K = \frac{\mu L V}{A P t} \tag{2.2}$$

in which K is the permeability, μ is the viscosity of the liquid, V is the total volume of the sample, L is the height of the sample, A is the cross-sectional area of the sample, P is the pressure gradient, and t is the recorded time.

[1] Milli Q is de-ionised water that has passed through a resin filter

2.1.3 Metabolite treatment

Direct treatment with metabolites as a proxy for excretions of microbes is used because sample treatment with live thermophile microbes is beyond the scope of this research due to temporal, budgetary, and logistical restrictions [2]. Thermophile microbes that can be present in geothermal, oil, and gas reservoirs can excrete a range of metabolites. For this study, the following range of metabolites are used: isobutyric acid, isovaleric acid, acetic acid, sodium sulphate, and sodium alginate. Where the sodium alginate and calcium chloride treatment mimics the presence of biofilm. Acetic acid is commonly excreted by sulphur reducing bacteria. Both isobutyric acid and isovaleric acid are excreted by microbes common in geothermal systems Sand [2003]. Sodium sulphate is added to provide sulphur for the formation of H_2S as would follow in the presence of SRB's.

In the set-up of the experiment, in-situ conditions of a geothermal reservoir are simulated, as described in chapter 1, within means of the project. The influence of the metabolites on porosity and permeability of the samples is expected to be mainly linked to temperature, concentration of metabolites, reservoir pressure, and initial rock properties (porosity, permeability, mineralogy).

Creating a pressurised and anaerobic environment is out of range of the possibilities of the laboratory equipment. The workflow described below is repeated for all temperatures and concentrations. The samples are dried in the oven to remove all water from the pores of the sample. A brine is prepared that has a similar chemical signature to what is found in sedimentary geothermal systems. Acetic acid, isobutyric acid, and isovaleric acid are added to the brine in such quantities that all acids are present at equal molarity. The pH of the solution is recorded. The samples are separately covered in sodium alginate and treated with calcium chloride, representing the presence of a biofilm. The samples are put into a beaker and immersed in the acidic solution and put into a shaker for 10 minutes to ensure there are no air pockets left in the samples. After shaking, the beakers are covered with equal sized sheets of aluminium foil and covered with a watch glass. Following this preparation, the samples are left to rest at temperature. After a week, the pH of the solution is recorded for each beaker. Then, 60 ml of acidic solution is pushed through a filter to remove solid material from suspension. 60 ml of Milli Q water is then added to the sample and the sample is shaken for 10 minutes. The vibrating motion

[2] Only special licensed laboratories are allowed to work with live microbes

should facilitate a replacement of the acid in the sample with Milli Q, as well as shake out loose solid material that might be present in the sample. Then once again, the liquid is pushed through a filter to remove solid material. This is repeated three times, so a total filtrate of 240 ml is formed and any solid material that has come out of the sample is caught in the filter. The samples are transfered to a clean beaker and left in Milli Q water. The samples are not oven dried immediately as salt from the brine is expected to precipitate and yield unrealistic values for porosity and permeability. Filters are oven dried until all water is removed before solid material is weighed.

Summarized, the workflow can be described as follows:

1. Dry samples in oven (24 hours, 105 Celsius)
2. Prepare brine
3. Mix metabolites to create acidic solutions (0.2[M], 1.0[M], 2.0[M]
4. Record pH of acidic solutions
5. Treat samples with sodium alginate and calcium chloride
6. Immerse samples in acidic solution and put in waterbath shaker for 10 minutes
7. cover samples with aluminium foil and watch glass
8. Leave samples in oven for 7 days
9. Record pH of acidic solution of all samples
10. Filter acidic solution and then re-immerse in milli Q water (repeat 3 times)
11. Extract samples and leave in milli Q water
12. Dry samples in oven (24 hours, 105 Celsius)

With a limited number of samples, and varying only a single parameter at once to investigate its influence on the process, it is opted to test a range of three temperatures and three concentrations as shown in Table 2.1.

Table 2.1: metabolite treatment scheme

	25 C	60 C	90 C
0.2 [M]	x1 x2 x3 y10	z1 z2 z3 x10	y1 y2 y3 x13
1 [M]	x7 x8 x9 x14	z7 z8 z9 x12	y7 y8 y9 y11
2 [M]	x4 x5 x6 z10	z4 z5 z6 x11	y4 y5 y6 z11

2.1.4 Peak strength

If a rock is damaged to an extent where the structural integrity of the rock is reduced, fracturing or compaction of the rock may occur. Since the experiment is not conducted under reservoir pressures, the influence of pressure is not yet represented in the experiment. Therefore, peak strength of the rock is measured. Fracturing and compaction of the rock can reduce intergranular porosity. However, it could create a secondary porosity and permeability. Peak strength measurements can not be performed on samples that are used for permeability and porosity measurements due to size restriction discrepancies between the methods. Therefore, peak strength measurements are done on dry cores that are have been treated with 1.0 [M] acid solutions at all three temperatures. Although peak strength of porosity and permeability measured samples can not be directly measured, the peak strength measurements of separate cores can provide an indication of the influence of pressure as an input parameter.

2.1.5 Final state

For determination of the influence that the metabolite treatment has had on the physical properties of the samples, a final state is recorded. Which is done by repeating the same measurements as for the determination of the initial state.

2.1.6 Thin sections

Five thin sections are made of samples both before and after laboratory experiments. Thin sections are examined under the microscope and changes in the mineralogy are described. Photo's are taken for every sample on 2.5, 5, and 10 orders of magnification.

2.2 Artificial Neural Network

Data obtained by the laboratory experiments are used to investigate whether a relationship can be found between in-situ conditions, initial physical parameters of the reservoir rock, and physical parameters of the degraded reservoir rock after the treatment as described in the subsection 'Metabolite Treatment' In this thesis, the open source Scikit-learn Python module [3] is used to investigate the relationship between initial porosity and permeability of the samples, the concentration of acid solution the samples are immersed in, and the environmental temperature. Scikit-learn provides simple tools for data sorting and machine learning applications. Machine learning problems are often divided into classification and regression problems. An explanation of the difference between classification and regression problems can be found in Appendix A in the section Neural Networks. Since the aim of this research is to predict continuous values for changing porosity and permeability of samples, this is a regression problem.

2.2.1 Train Test Split

A neural network has to be trained with 'training data' to learn the rights output parameter for a certain combination of input parameters. Splitting the dataset into two subsets, one subset can be used to train the model and acquire a best fit for the training data (27 samples). The other subset can be used as a test dataset to validate the performance of the model (9 samples). Machine learning algorithms perform best with large amounts of data (more than 1000 data points). When data sets are small, multiple instantiations of the train test split can be used to optimise training of the model on the available data Demuth et al. [2014]. This means that the total data set is split up in 27 training data points and 9 test data points in multiple different ways.

2.2.2 Approaches

Both a simple linear regression algorithm and a multi-layer perceptron approach are used. The linear regression algorithm minimises an ordinary least squares function and forms a prediction based on the linear relationship that has been found in the training

[3] all software used in this thesis can be found on the sci-kitlearn.org website with accompanying explanations on how to install and use the software. This thesis has used python2.7 in a jupyter notebook environment

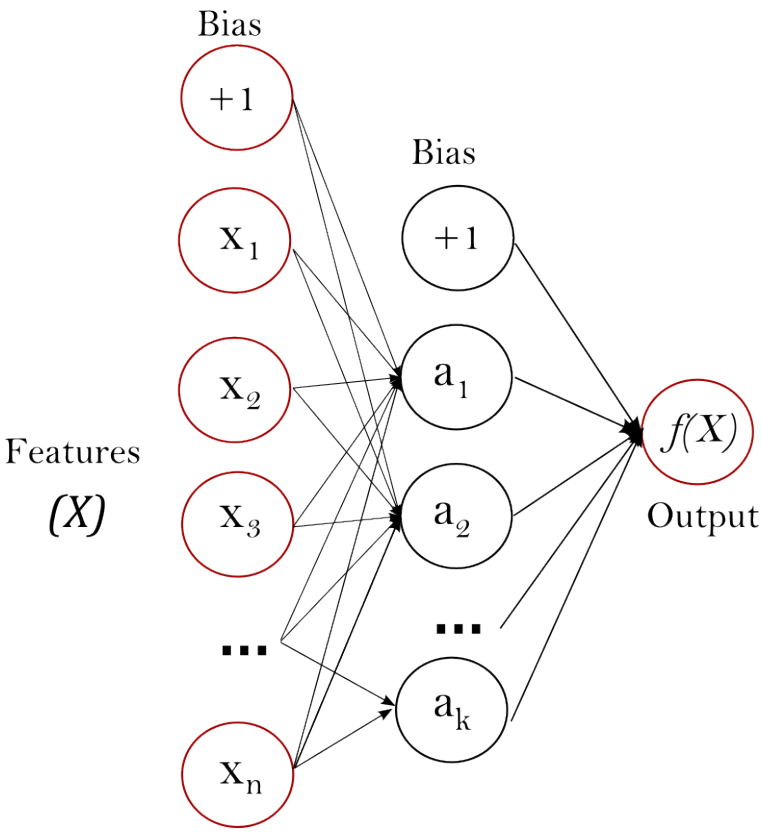

FIGURE 2.1: Single Hidden Layer Multilayer Perceptron with a Bias Neuron (scikit-learn.org)

data. A Multi-Layer Perceptron (MLP) can be used, which estimates an output (f(X)) from a set of inputs, where the number of input neurons is equal to the number of input variables. Hidden layers perform non-linear transformations of the input values, which allows the algorithm to find non-linear relationships between input and output. Weights between neurons are then adjusted in iterations to minimise a loss function. This multi-layer perceptron implementation uses a square error loss function. The input neurons that have the largest weights to the hidden layer after conversion of the model are the most influential in the prediction result. A visual representation is given in Figure 2.1. The Multi-Layer Perceptron Regressor in Scikit-learn allows for the use of a set of different solvers. Since the data set is small, it is opted to use the 'l-bfgs solver'. The l-bfgs solver is a quasi-newton method algorithm and uses the first and second derivatives of the loss function to steer its optimisation. A thorough mathematical explanation of this solver can be found in Liu and Nocedal [1989]

2.2.3 Fine-tuning

All neural networks need to be fine-tuned to show good results. There are several rules of thumb that are followed in this research. Firstly, most neural networks only have a single hidden layer. It is suggested that problems that require more than one hidden layer, and thus need more than one non-linear transformation, are too complicated to solve with a neural network Demuth et al. [2014]. Secondly, the number of neurons needed in the hidden layer follows from equation 2.3.

$$N_h = \frac{N_s}{\alpha * (N_i + N_o)} \tag{2.3}$$

In which N_s is the number of samples, N_i is the number of input neurons, N_o is the number of output neurons, and α is an arbitrary scaling factor within the range 2-10. The number of neurons in the hidden layer are usually trimmed down to contain the least number of zero-weighted connections in accordance to Ockham's razor Demuth et al. [2014].

2.2.4 Validation

Performance of predictions can be quantified through the R2 metric. The R2 metric measures the squared error difference between a model, and a mean model (also called worst model) on a scale of 0.0 - 1.0 The optimal score is 1.0, where a model would reflect reality perfectly. A network that predicts a constant mean value without consideration of input parameters will score 0.0. Thus, the R2 metric portrays on a scale between 0 and 1 how well the model performs compared to a perfect model, and a mean model as visualised in Figure 2.2 . A score can also be negative when a Network prediction is worse than a constant mean value. Since there is a small sample size, it is not expected that the neural network will perform very well. Performance of the neural net should improve when more data points are added. To quantify the expected improvement of this particular neural network, the neural network can be trained with a standard data set for regression problems: The Boston housing market data set. This comparison in performance could provide insight into an expected improvement in performance of the neural net if more samples are added.

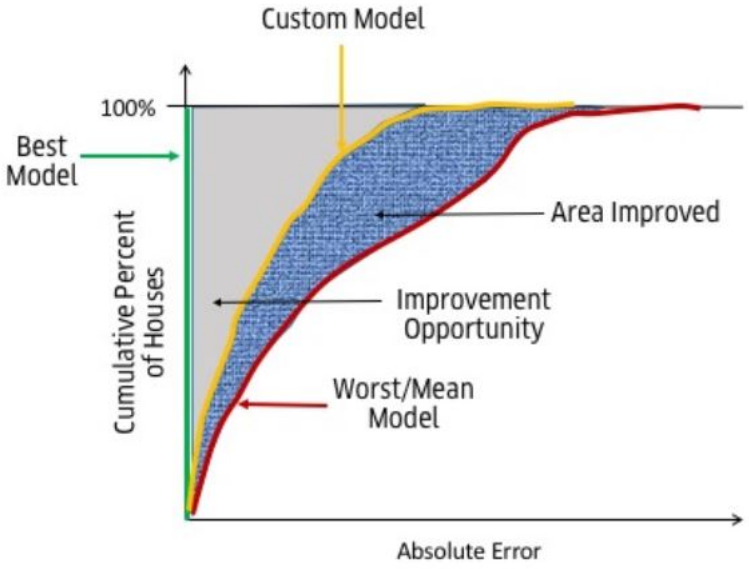

FIGURE 2.2: Visualisation of the meaning of the R2 metric (Ragriwal, 2017)

Chapter 3

Results

3.1 Initial permeability and porosity

Dry porosity, wet porosity, dry permeability, and wet permeability have been recorded for all samples before and after metabolite treatment is executed. The full set of measurements can be found in Appendix B in Table B.1. Porosity and permeability measurements of Bentheimer Sandstone before laboratory experiments agree well with literature as found in Peksa et al. [2015]. The wet and dry permeability in the direction parallel to the bedding planes is lower than perpendicular to the bedding planes. Wet permeability is more variable in the y-direction than in the x- and z-directions as seen in Table 3.1.

TABLE 3.1: Initial values and standard deviations for porosity and permeability

	average p dry (%)	stand. dev. p dry (%)	average perm dry (D)	stand. dev. perm dry (D)
x	0.270615353	0.010183603	2.669314091	0.2612604
y	0.266177117	0.003183197	2.376778338	0.217456994
z	0.263494399	0.003438369	3.010324266	0.327303765
	average p wet (%)	stand dev p wet (%)	average perm wet (D)	stand. dev. perm wet (D)
x	0.24798524	0.005857355	1.301731347	0.101940781
y	0.251098795	0.004080874	1.268676122	0.209001287
z	0.25190471	0.003668893	1.683681723	0.078825586
	unit density kg/m3	unit weight kN/m3		
x	1.984374725	19.46671605		
y	1.982247963	19.44585252		
z	1.979591087	19.41978856		

3.2 pH changes

Acid solutions in which the samples are treated are at 0.2, 1.0, and 2.0 M and have pH values of 2.13, 1.83, and 0.95 respectively before sample immersion. pH values changed during the experiment. Average pH values and their changes are given for each concentration and temperature combination in Table 3.2. Table 3.2 shows that pH decreases in the 25 °C and 60 °C environments apart from the 25 °C and 1.0 [M] environment and at 90 °C, pH increases for all concentrations.

TABLE 3.2: average pH before experiment, after experiment, and pH change for each tested environment

	25°C	60°C	90 °C
0.2 [M]	2.13; 1.89; -0.24	1.83; 1.53; -0.31	0.95; 1.10; 0.15
1.0 [M]	2.13; 2.39; 0.26	1.83; 1.67; -0.16	0.95; 1.17; 0.22
2.0 [M]	2.13; 1.87; -0.26	1.83; 1.28; -0.56	0.95; 0.97; 0.02

3.3 Sample mass

Weight of the samples changes throughout the experimental process by addition of sodium alginate, the dissolution of existing material, and precipitation of new material. A full overview of the sample weights in all stages of the experiment can be found in Appendix B in Table B.3.

3.3.1 Sodium alginate

Addition of sodium alginate and calcium chloride to mimic a biofilm has added weight to the samples. Any differences in quantities of sodium alginate applied to the samples has been documented and is given in the overview in Appendix B in Table B.3. Differences in alginate addition between samples do not show a relationship to permeability and porosity changes.

3.3.2 Filter weights

After immersion of samples in acid and being left at their respective temperatures for a week, acid is extracted and put through a filter. The sample is re-immersed in Milli-Q, waterbath shaken, and the fluid is filtered 3 more times. Weight added to the filter can be assumed to be solid material lost by the sample during the procedure. Filter weights show that samples lose between 0 and 1 gram of solid material during the experiment.

3.3.3 Final weight

At the end of the laboratory experiment, all samples except for samples y3, y4, y5, and y6, show very small changes in weight, within measurement error (under 0.1 g). Sample y3 has been heated at 90 °C at 0.2[M] , and is a sample that has lost all solution in the process due to incomplete closing of the beaker. Sample y4, y5, y6 have been exposed to 90°C at 2.0 [M]. The added weight in y6 is due to halite crystals forming on top of and inside the sample. For samples y4 and y5, there were no visual differences with samples that have not shown added weight.

3.4 Final porosity and permeability

Presented in this section are graphs that visualize the initial porosity and permeability of the samples as well as the changes due to the laboratory experiments.

The dry porosity of the samples has decreased for all concentrations and temperatures (between about 0-10%). The wet porosity of the samples decreased as well with similar quantities. Permeability however, decreased more significantly (mainly between 20-40%) at all concentrations and temperatures as presented in figures 3.3 3.6 3.12.

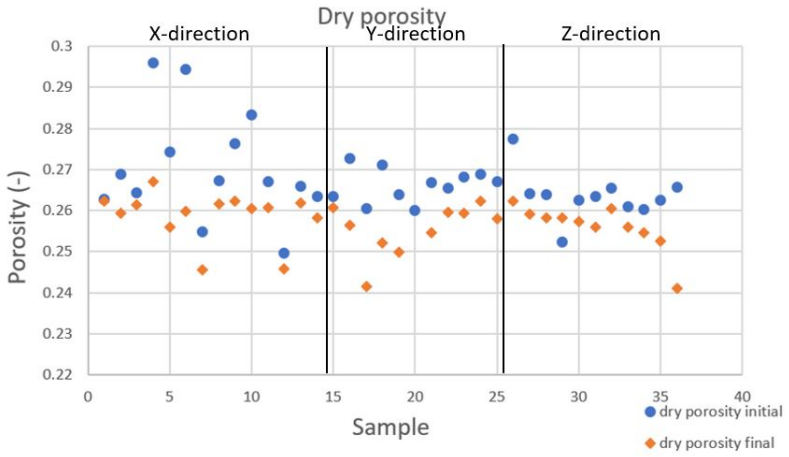

FIGURE 3.1: Dry porosity before and after metabolite treatment

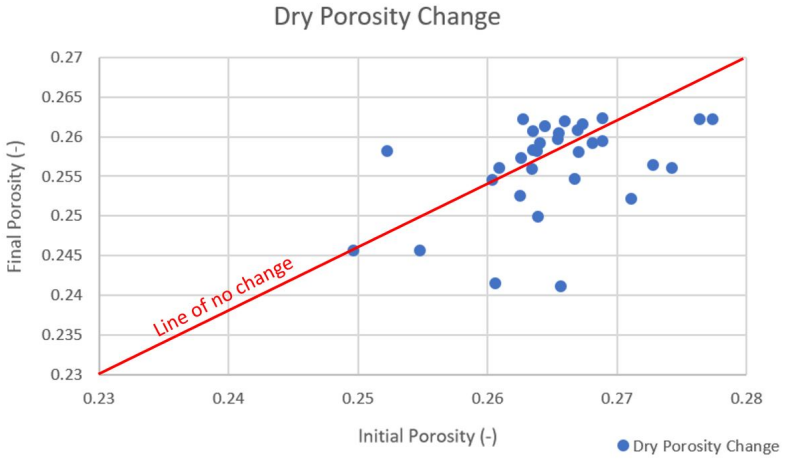

FIGURE 3.2: Initial dry porosity vs. final dry porosity

FIGURE 3.3

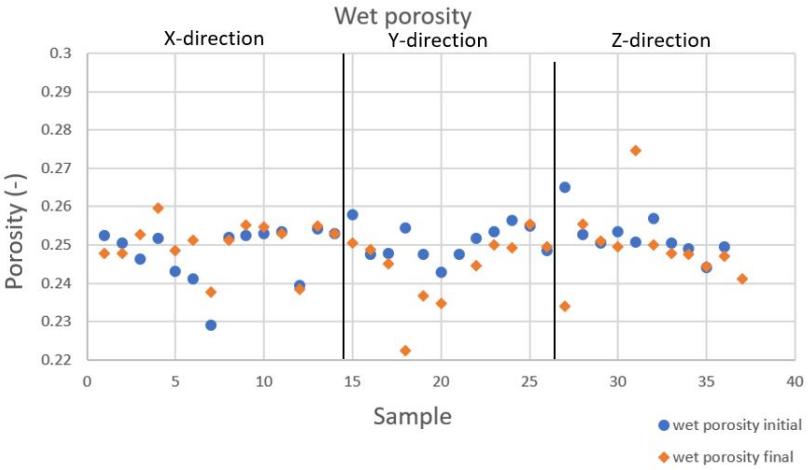

FIGURE 3.4: Wet porosity before and after metabolite treatment

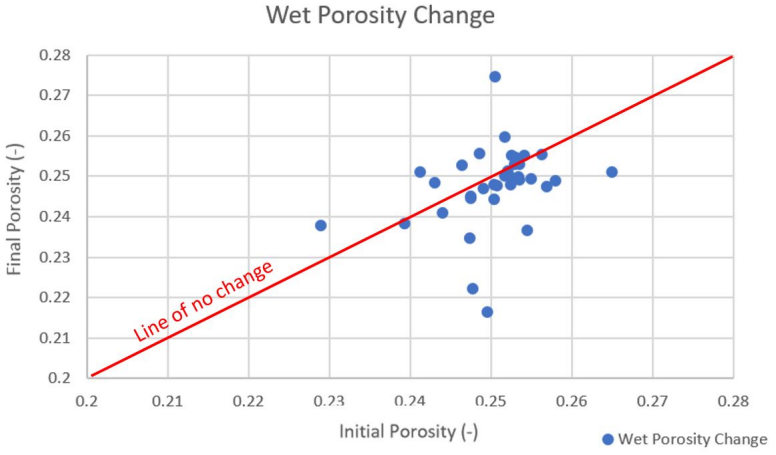

FIGURE 3.5: Initial wet porosity vs. final wet porosity

FIGURE 3.6

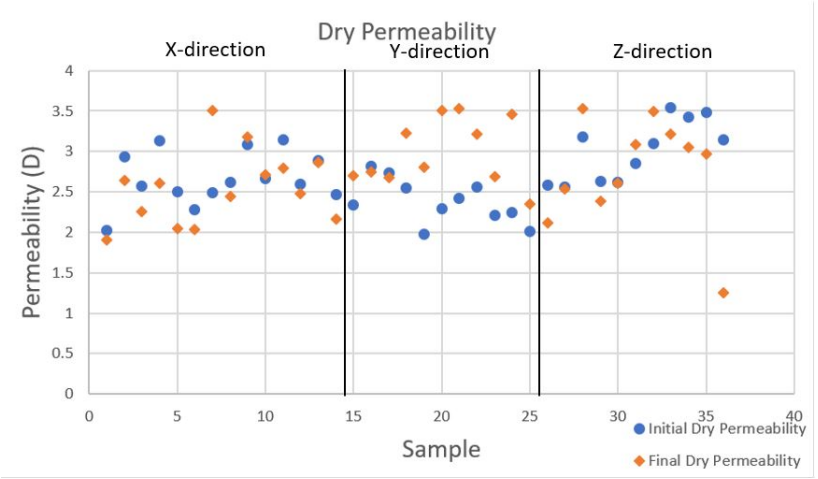

FIGURE 3.7: Dry permeability before and after metabolite treatment

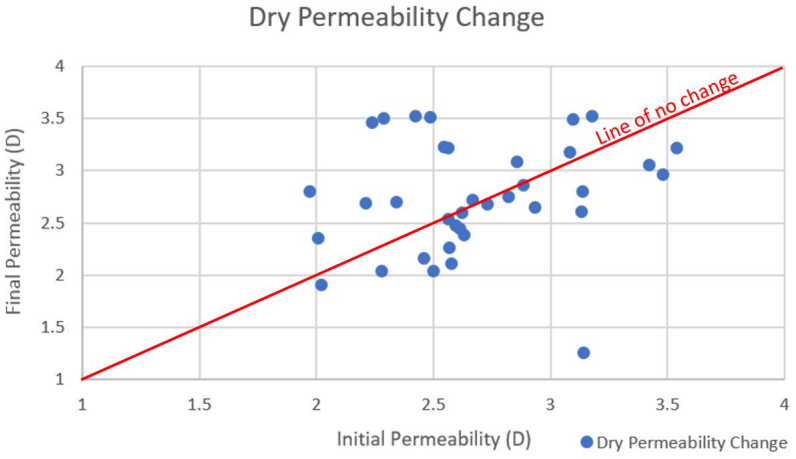

FIGURE 3.8: Initial dry permeability vs. final dry permeability

FIGURE 3.9

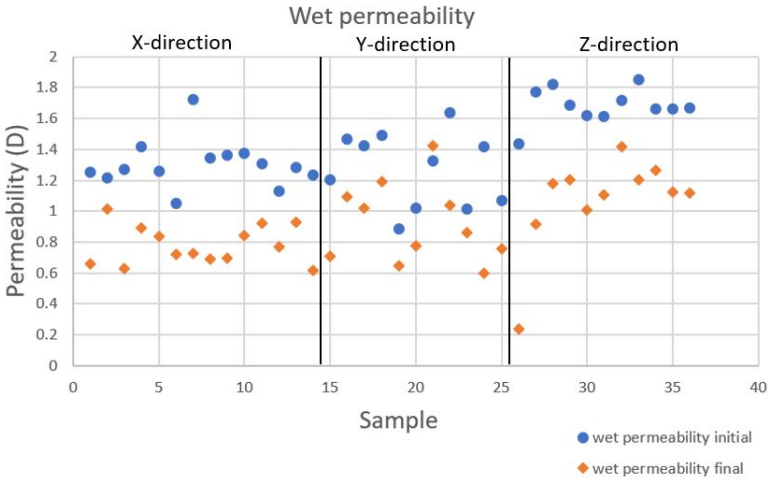

FIGURE 3.10: Wet permeability before and after metabolite treatment

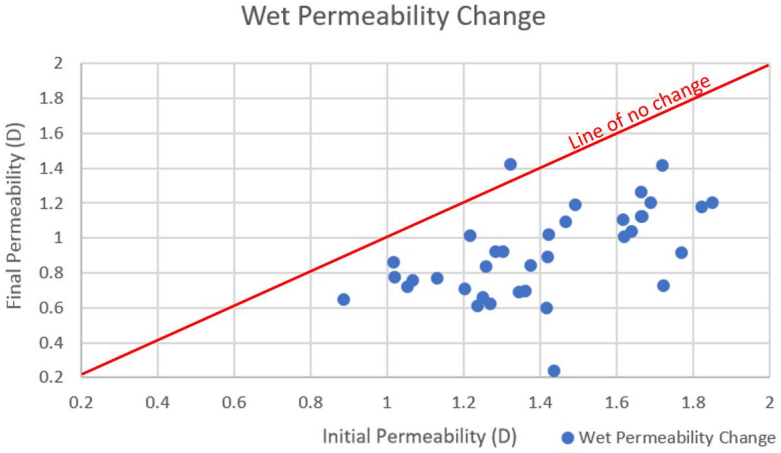

FIGURE 3.11: Initial wet permeability vs. final wet permeability

FIGURE 3.12

3.5 Peak strength

Peak strength measurements are performed on both treated and untreated Bentheimer sandstone samples. Full data on peak strength measurements can be found in Appendix B. Peak strengths for dry Bentheimer Sandstone samples that have been subjected to the acid solutions have an average peak strength of 31.24 MPa, as presented in Table 3.3. This is lower than the 38.93 MPa as found for dry Bentheimer Sandstone in literature

Peksa et al. [2015]. However, peak strength measurements have to be done on untreated Bentheimer Sandstone samples from the same block as treated samples were sourced from to verify decrease in peak strength.

TABLE 3.3: Peak strength values for microbially degraded Bentheimer Sandstone cores

Sample	Peak Strenght (MPa)
Ya	30.9390
Zb	29.0261
Zc	31.3705
Zd	29.7443
Zf	35.1389

3.6 Thin sections

Thin sections of untreated Bentheimer sandstone show matching results with Peksa et al. [2015]. Bulk majority of minerals is silicate with occasional feldspar and kaolinite. Cement is made up of quartz. Figure 3.13 shows a thin section of fresh Bentheimer Sandstone. Grains are quartz and minor occurence of clay minerals (kaolinite) is seen. Figure 3.14 presents a thin section of metabolite treated Bentheimer Sandstone. Red rectangles indicate areas where grains appear to have solid material coming loose and releasing into the pore space. Figure 3.15 shows a close up of loose material in pore space.

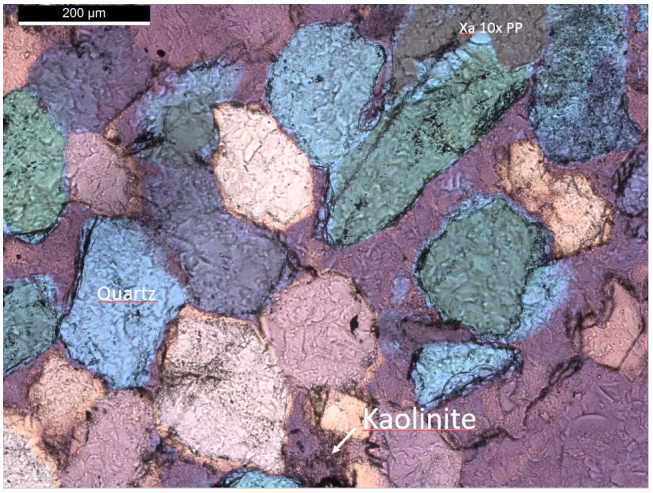

FIGURE 3.13: Sample x1 10 times enhanced

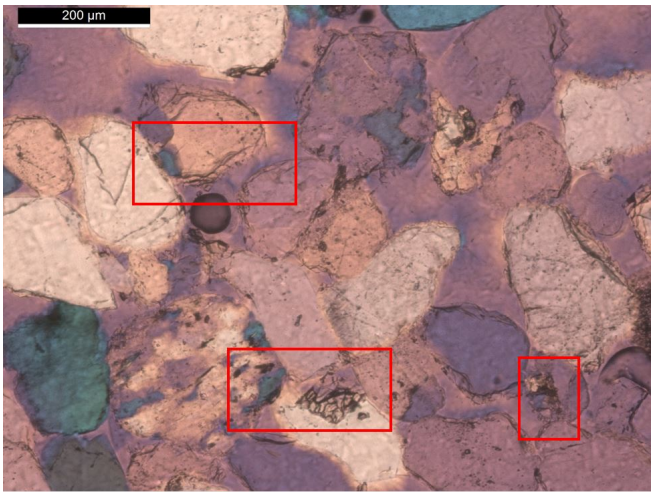

FIGURE 3.14: Sample Y5 10 times enhanced

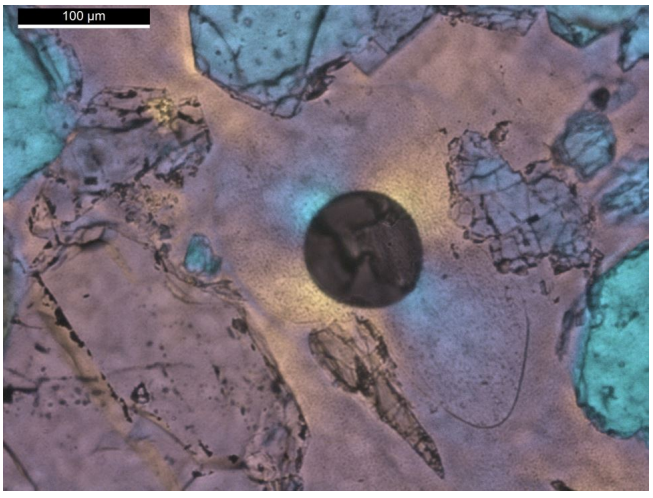

FIGURE 3.15: Sample Z5 20 times enhanced

3.7 Flow reversal

If fines exist in the pore space of samples and clog pore throats within a single dominant flow direction, it could be expected that the fines should be moved out of pore throats when flow direction is reversed. As such, the permeability measurements should show a decreasing trend over the first few measurements until fines are again stuck in pore throats, this time in the other direction. Flow reversal has been performed in wet permeability measurements and the results are shown in Figure 3.16. Permeability measurements decrease and stabilize over four consecutive measurements.

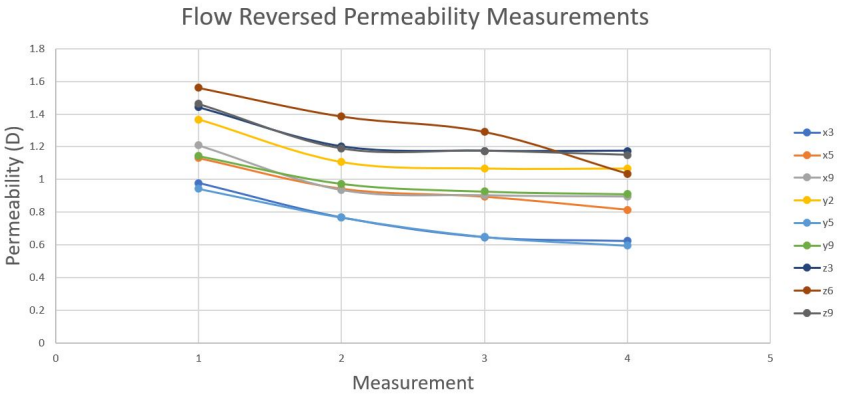

FIGURE 3.16: Wet permeability measurements after reversal of flow direction

3.8 Neural Network

The python scripts associated with this chapter can be found in Appendix C.

3.8.1 Multi-layer Perceptron

The Multilayer Perceptron has 1 hidden layer of 4 neurons, uses the 'tanh' activation function as a non-linear transformation and an 'l-bfgs' solver to steer model optimisation. Input parameters are initial wet porosity, initial wet permeability, temperature, and concentration for the prediction of wet porosity and wet permeability. The number of input parameters has been restrained to 4 as an increased number of input parameters with the used sample size decreases accuracy of the neural network. For a sample size of 36, multi-layer perceptron results show a decent prediction ability for wet permeability as presented in figure 3.17. The Neural Net appears to have a slight bias to overestimate wet permeability. Extreme measured values are not predicted well. The R2 score of the multilayer perceptron of several instantiations of the train-test-split fall in the range 0.32-0.35. R2 values for each prediction are given at the bottom of their respective figures.

From the same data, it is attempted to predict wet porosity. Results for wet porosity prediction are shown in Figure 3.18. he Neural Net has a consistant bias for overestimation of wet porosity. R2 values for wet porosity prediction in this multi-layer perceptron for several instantiations of the train-test-split are all in the range 0.0 - 0.1

Predictions for dry porosity and dry permeability use initial dry porosity, initial dry permeability, temperature, and concentration as input parameters. Prediction of dry porosity reaches a similar result with R2 values between 0.0 and 0.1 as shown in Figure 3.20. Prediction of dry permeability similarly does not perform very well with R2 values in the range 0.1-0.2 as presented in Figure 3.19.

Weights between neurons of the multi-layer perceptron are recorded to determine which parameters have the largest influence on porosity and permeability changes. The full tables of weights between neurons can be found in Appendix B in Table B.5. For both dry and wet permeability predictions, initial porosity values have the largest influence. For both dry and wet porosity predictions, temperature appears to be the most significant parameter. Initial porosity and initial permeability have slightly lower weights than temperature.

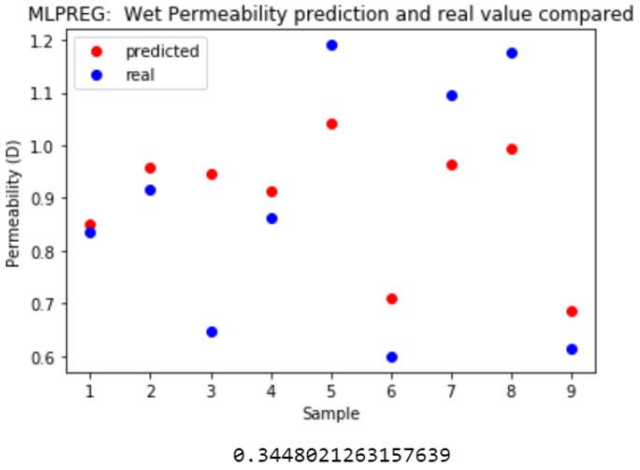

FIGURE 3.17: Multi-layer Perceptron predictions for wet permeability

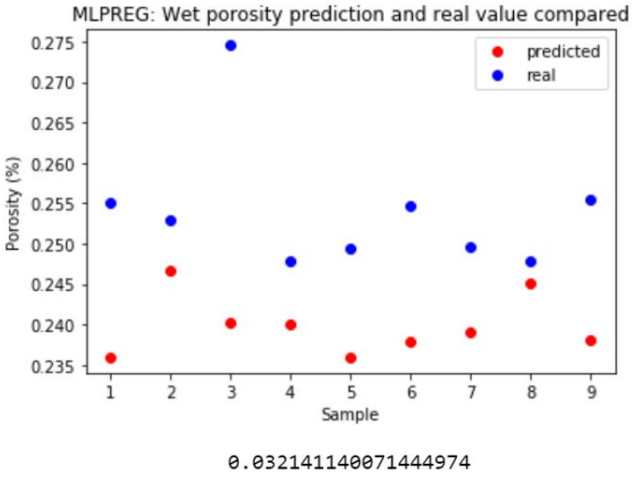

FIGURE 3.18: Multi-layer Perceptron predictions for wet porosity

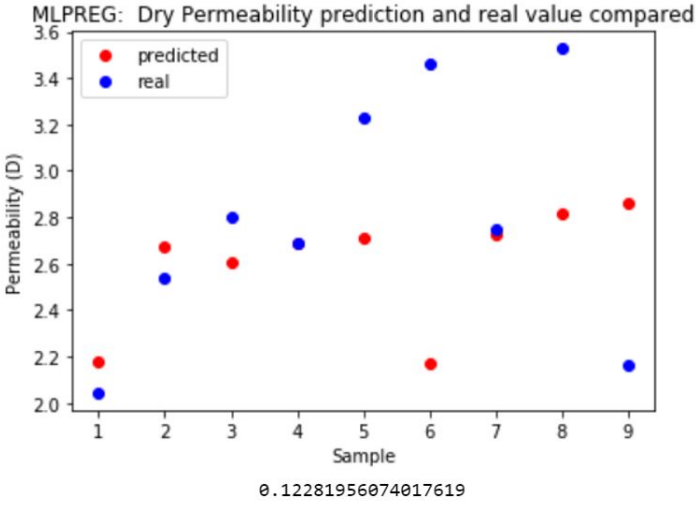

FIGURE 3.19: Multi-layer Perceptron predictions for dry permeability

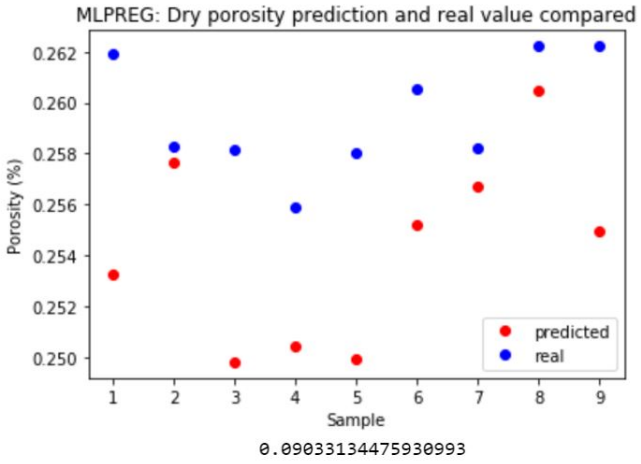

FIGURE 3.20: Multi-layer Perceptron predictions for dry porosity

3.8.2 Linear Regression

Results from a least squares linear regression model for prediction of wet permeability, wet porosity, dry permeability, and dry porosity are shown in figures 3.21, 3.22, 3.23 and 3.24 respectively. Results from linear regression in terms of R2 values are similar to multi-layer perceptron and are shown at the bottom of their respective figures.

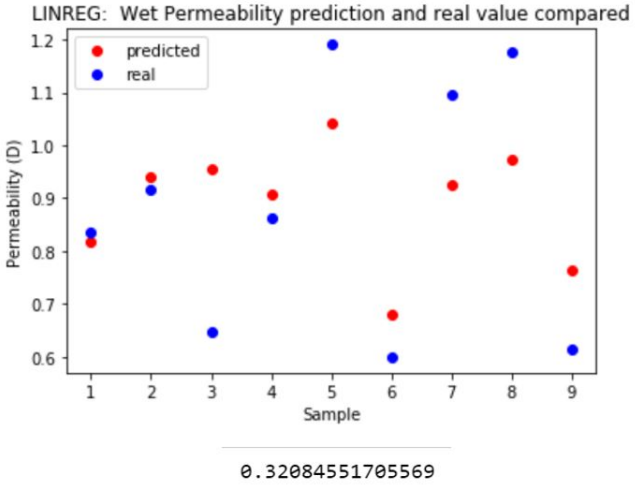

FIGURE 3.21: linear regression predictions for wet permeability

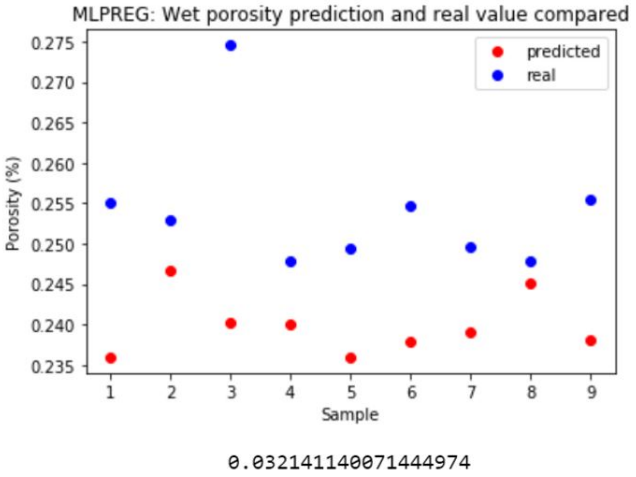

FIGURE 3.22: linear regression predictions for wet porosity

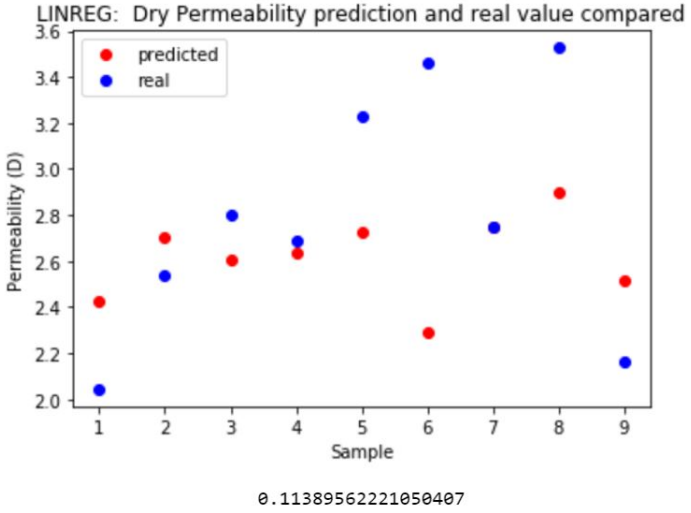

FIGURE 3.23: linear regression predictions for dry permeability

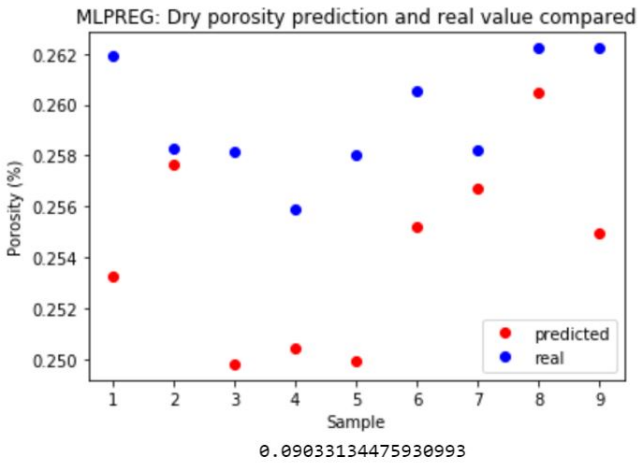

FIGURE 3.24: linear regression predictions for dry porosity

3.8.3 Validation

The same Multi-layer Perceptron and linear regression models have been applied to the Boston Housing Market Data Set for 36, 70, 150, and 500 data points to measure performance of the models with increasing sample sizes. The data set uses the same number of input parameters and predict the mean value of real estate in Boston. Here, for the sake of brevity only R2 values of the models are presented as seen in Table 3.4. R2 values decrease with sample size for the linear regression model while R2 values for the multi-layer perceptron improve with sample size.

TABLE 3.4: R2 values for predictions of the mean real estate values of the Boston Housing Market Data Set with sample size

NO. SAMPLES	R2 LINREG	R2 MLP
36 samples	0.737	0.756
70 samples	0.728	0.751
150 samples	0.615	0.776
500 samples	0.480	0.792

Chapter 4

Discussion

4.1 Porosity and Permeability Changes

The overall trend in all metabolite concentration and temperature environments is a slight decrease in porosity and a more substantial decrease in permeability of the samples. Moreover, wet permeability temporarily increases when flow is reversed in wet permeability measurements. One way to explain temporary increase in permeability after flow reversal is the presence of loose solid particles in pore space that are pushed into narrow pore connections and blocking openings. Fines clogging pore throats is a known cause for formation damage in the context of fluid injection where there are solid particles in suspension in the injected fluid Engler [2010]. In-situ mobilisation of fines is a process decribed in publications by Krueger et al. [1988] and Wojtanowicz et al. [1988]. Through the shaking procedure and flushing of the sample before metabolite treatment, it can be assumed that possible loose solid particles are created during metabolite treatment. Loose particles could either been eroded from existing grains, in which case it would not impact the overall pore volume of the sample. Another explanation could be that loose material has precipitated from the brine during the experiment Sand [1997].

4.2 Thin Sections

Thin sections show an increase in loose material in the pore space, but no strong differences are identified in mineralogy. Loose material seen in thin sections are made of

quartz. As such, loose material could originate from original grains as shown in Figure 3.14 No porosity and permeability analysis has been done on the thin sections due to time constraints, but this could yield insight into the cause of permeability decrease. Porosity and permeability analysis could image whether effective permeability is largely reduced by clogging of large areas causing dispersed flow or if effective permeability is reduced by narrowing of pore throats throughout the sample.

4.3 Peak Strength

Peak strength of Bentheimer Sandstone cores that have been immersed in 1.0[M] acid solution has decreased equally at all three temperatures. Peak strength reduction could be caused by degradation of the contact surfaces between sand grains within the sample. As thin sections show some degradation of grain surfaces, this could have impacted the peak strength of samples where contacts between grains are more easily broken. It should be noted that only 6 metabolite treated cores have been measured, which is not enough to draw definite conclusions.

4.4 Neural Network

R2 scores for the neural network fall in the range 0.0-0.35. In natural sciences, scores R2 above 0.6 are usually required to adequately support any interpretations made from the performance of the neural network (In social sciences, neural networks with R2 scores of 0.1 can already yield insight due to the highly variant nature of for example human behaviour). However, scores up to 0.4 do provide insight into parameter influences Demuth et al. [2014]. It is expected that neural network performance should improve with growing sample size, as is the result from the Boston Housing Market Data set. Additionally, when more samples are added and more parameters are measured such as pressure, major mineral content, O_2 content, and CO_2 content, more influential parameters could be identified and improve the performance of the network. This has not been done in this research due to restrictions in the lab.

Permeability decrease tends to be larger for samples that have a small initial porosity. Small initial porosity usually translates to smaller pore throats, which subsequently will

clog more easily than large pore throats. Additionally, precipitation of solid material will have a larger effect on permeability in small pores as flow will be restricted more easily. Still, the trend is based on a small sample size with a weak relationship and large variance between samples.

4.5 Methodology Improvements

The laboratory methodology used in this research is aimed to be a first protocol to be improved upon in future research. The range in environments could be extended to explore threshold values for different mineral precipitation and dissolution behaviour. Improvements to the methodology could be the introduction of an autoclave which would allow the simulation of an anaerobic in situ environment under pressure.

Chapter 5

Conclusions

5.1 Conclusions

Metabolite treatment of Bentheimer Sandstone samples under a range of acidic and temperature environments has shown a significant decrease in permeability and a slight decrease in porosity from their original state. Thin sections show no major changes in mineral composition, but small solid particles are coming loose from grain surfaces. Fines present in the pore space could be mobilised in situ from existing grains. Flow reversal in liquid permeability measuremernts shows a continuous decrease in permeability measured in subsequent measurements, pointing towards pore throat clogging by fines. Peak strength of Bentheimer Sandstone cores exposed to 1.0[M] metabolite solution at 25, 60, and 90°Celsius, is measured at an average of 30 MPa. A multi-layer perceptron achieves up to 0.34 R2 values for prediction of wet permeability of exposed samples. Prediction of dry permeability performs with an R2 value in the range 0.1-0.2. Both dry and wet porosity predictions only reach R2 values up to 0.1. The multi-layer perceptron performs similarly to an ordinary least squares linear regression model but validation with an alternative data set shows better performance for the multi-layer perceptron with increased sample sizes. The neural network allows for early identification of important controlling factors which allows for targeted investigation of their impact. Weights between neurons associated with input parameters show that wet and dry permeability are mainly influenced by the initial wet and dry porosity respectively.

5.2 Recommendations

Further research could perform laboratory experiments with metabolites under pressure and expanded range of temperatures. Additionally, anaerobic environments could be simulated. CO_2 injection could be used to accurately mimic CCS environments. More data points could be added to improve the performance of the neural network and more clearly identify the most influential factors that result in porosity and permeability change of reservoir rock. The research could be widened to include other types of sedimentary rock with different mineral assemblies and initial values for porosity and permeability. Major mineral content could subsequently be added as an input parameter into the neural network.

Appendix A

Literature Review

A.1 Introduction

This literature review provides background information for the research on microbial reservoir degradation in geothermal and CCS (Carbon Capture and Storage) settings in this thesis. Previous research on microbial degradation has been focused on degradation of petroleum products and exploitation infrastructure such as pipelines. Research on reservoir properties is focused on, for example, water-rock mass interaction, fines impairment, and fluid injection incompatibilities. However, microbial degradation mechanisms for corrosion of reservoir rock mass has not been widely researched. With regard to research in this thesis, it is useful to briefly review existing literature on the following topics:

1. Characteristics of geothermal and CCS environments
2. Movement of microbes within reservoirs
3. Microbial degradation of organic and inorganic substrates
4. Sandstone corrosion
5. Formation impairment
6. Methods for permeability and porosity measurements
7. Methods for confining strength measurements

8. Bentheimer sandstone characteristics

9. Artificial Neural Networks for rock mechanics

A.2 Characteristics of geothermal and CCS environments

Geothermal systems are characterised in three groups in the literature. Volcanic geothermal systems, convective systems in tectonically active areas, and sedimentary systems with permeable layers at great depth Saemundsson et al. [2013]Bövarsson [1964]. In sedimentary systems, reservoir fluids are commonly brines and temperature is dependent on the depth of the reservoir. In low temperature systems, temperatures do not exceed 150C Saemundsson et al. [2013]. An overview of classifications of geothermal systems is presented in table 1 Bövarsson [1964]. In most geothermal fluids , minerals, silica, and salts are only found in the liquid and solid phase. CO_2 can be dissolved in the liquid . Oxygen is usually very low in concentration Gunnlaugsson et al. [2014]. Dissolved elements in geothermal waters can either originate from water-rock interactions and include Si, Al, Na, Ca, K, Mg, Fe, Mg, and Mn. Gunnlaugsson et al. [2014].

Storage reservoirs for Carbon Capture and Storage projects are usually depleted oil or gas reservoirs or deep saline aquifers and as such are sedimentary in nature Bertier et al. [2006]. Research has been done on exploiting co-produced geothermal resources from petroleum reservoirs (e.g.: Barbacki [2000] Liu et al. [2018], Singh et al. [2017]).

A.3 Movement of microbes in porous media

Microbial processes in porous media have been researched in detail for drinking water protection and contamination remediation (e.g.: Corapcioglu and Haridas [1985], Clement et al. [1997]). Many laboratory experiments have been conducted to investigate the transport of microbes through porous media. However, results of laboratory experiments are hard to generalize due to the complex nature of natural and engineered systems and their chemical, physical and biologically heterogeneity. Whereas the initial penetration of a rock by microbes is mostly dependent on porosity and permeability, transport of microbes through porous media is dependent on many factors including: Size and shape of microbes Size and shape of rock grains Presence of minerals as e.g.

Iron Oxide Porosity of reservoir rock Permeability of reservoir rock Adsorption rates Detachment rates Microbial growth and inactivation Particle sedimentation distribution Tufenkji [2007]

A.4 Microbial Degradation/Corrosion of Organic and Inorganic Material

Microbial degradation of organic and inorganic substrates has been widely researched (Sand [1997], refs??). Microbes can degrade quality of petroleum products and corrode production pipelines. Degradation of inorganic substrates can happen through mineral acids, organic acids and organic solvents among others. Organic solvents might cause dissolution of natural material to a point where structural integrity of the rock is diminished Sand [1997]. Organic acids can, as well as acidic action , make metal ions complex and make normally insoluble compounds prone to dissolution. Finally, the growth of biofilm can promote growth and activity of SRB, which may lead to increased hydrogen sulphide biocorrosion Sand [1997]. Examples of acids that can cause corrosion of inorganic substrates are acetic acid and butyric acid. Hydrogen sulphide can also lead to reservoir plugging due to the precipitation of metal sulphides Magot et al. [2000].

A.5 Summary Microbial Processes in Porous Media

When researching microbial degradation of reservoir rock, it is required to understand microbial presence in reservoirs and the chemical processes that accompany such presence. Therefore, it is necessary to combine knowledge on microbial transport in porous media and degradation of inorganic substrates. Coupled processes reactive transport models have been attempted where physiochemical processes as advection, dispersion, diffusion, and straining have been described in combination with biological processes such as growth/decay, sorption and adhesion and multiple rates of reactions. Other processes that are of influence include pore clogging by microbes, sedimentation of microbes, and the formation of biofilm structures on individual grains of the host rock Murphy and Ginn [2000]. Complexity of these processes makes it difficult to accurately simulate the transport of microbes through porous media while describing the effects of microbial

presence on permeability and porosity. Thus, microbial transport in porous media and degradation of reservoir rock are highly complex phenomena with many interdependent processes that are often case specific. This leads to an inhibition to generalize experimental data for modelling purposes. Still, fundamental controls on microbial transport and degradation are increasingly well known.

A.6 Bentheimer Sandstone characteristics

As the research will use Bentheimer Sandstone is to be used create afor the data set for microbial degradation in this research, it is useful to explore previous research on the specific formation. Significant previous research has been done on the properties of the Bentheimer Sandstone, which has been summarized and elaborated upon by Peksa et al., 2015 Peksa et al. [2015]. Bentheimer Sandstone used in this paper are collected from the Romberg Quarry in Gildehaus, Germany. Below, relevant information on the Bentheimer Sandstone is imported from Peksa et al. ,2015. The Bentheimer Sandstone consists of 91.70 wt quartz, 4.86wt feldspar, 2.68wt clay minerals, and 0.17wt pyrite and iron hydroxides. Kaolinite causes some pore clogging. Quartz overgrowths are the main reducers of intergranular porosity . Porosity is determined to be in the range 0.23-0.27 vol. However, the range narrows significantly between samples taken from the same block. It is stabled by Ultra Pycnometer, gravitational method and image analysis. There are minor discrepancies between the findings of each method but within the range of error. Liquid permeability has been tested in flow experiments. Permeability is in the range 1.35 3.09 Darcy, with an average of 1.80 Darcy.

A.7 Sandstone Corrosion

CO_2-water-rock interactions can play a significant role in the dissolution of rock. CO_2 can be present in geothermal brines and is highly present in CCS environments. Mineral precipitation due to CO_2-water-rock interactions can decrease permeability Shiraki and Dunn [2000]. Dissolution and precipitation of carbonates and Al-silicates have a significant impact on reservoir properties Bertier et al. [2006]. pH of the fluid is important for the rate of Si dissolution. Not only total solubility but also rates of Si dissolution are important as it determines the distance away from a well at which dissolution can still

occur Reed et al. [1980]. Silicate weathering reactions in solutions can vary by several orders of magnitude over a 100C temperature range Lasaga [1981]. Dissolution rates of silica show a relation to ionic strength. The weathering sequence of minerals in an anaerobic, microbially controlled system is almost opposite to the Goldich Weathering Sequence in which quartz takes longer to dissolve than other silicates as olivine and plagioclase Bennett et al. [2001].

A.8 Formation Impairment

Formation impairment is the term for a reduction of permeability and effective porosity of a reservoir during production or injection. Several factors can cause formation impairment. One of which is fines impairment. Small particles may be reintroduced into the reservoir at a reinjection well which can cause pore clogging. Small particles can also be generated by interaction between host rock and reservoir fluid. Precipitation of minerals from the reservoir fluid can decrease effective porosity and permeability of the reservoir in the vicinity of a well Krueger et al. [1988]. Although introduction of small solid particles is beyond the scope the microbial reservoir degradation research, known mechanisms of formation damage are of interest to analysis of permeability and porosity of a reservoir rock. the possibility should be considered that during the experiment, small solid particles are released from the host rock in a reaction with metabolites, leading to pore clogging. Effects of solid particle pore clogging could be investigated by flow inversion during permeability measurements Engler [2010]. Precipitation of minerals from the brine could also occur.

A.9 Methods for Porosity and Permeability Measurements

To accurately measure the effects of metabolic treatment of sandstone samples, initial and final porosity and permeabilities need to be established. For measurements of porosity and permeability, a range of methods exists. Measuring dry porosity using a gas expansion Ultra Pycnometer uses Boyles gas expansion law Peksa et al. [2015]. The method yields the effective porosity and bulk density of the sample. Wet porosity can be measured by submerging the sample in liquid and following Archimedes law. Dry

permeability can be measured with N2 and a gas permeameter. Absolute wet permeability can be calculated using flow velocities and pressure differential measured with a liquid permeameter using Darcys law Peksa et al. [2015]. A different method that can yield both porosity and permeability is the CT-scan of a sample. Permeability can also be measured under confined conditions. Permeability can respond to axial pressure and radial pressure. Increasing confin pressure is found to be the main mechanism for water permeability reduction (Voorn et al., 2014)

A.10 Artificial Neural Networks for rock mechanics

In the case of microbial reservoir degradation, high interdependence and complexity of degradation mechanisms makes it difficult to accurately model the process from first principles . Instead, it can be considered to identify significant impactors of the process and to find complex relationships between an impactor and the final physical parameters of the sample. Neural Networks can be used to predict the outcome to a certain problem assuming there is a complex relationship between the outcome and the many drivers of a process. In previous research, Neural Networks have been applied for fractured reservoir characterisation Ouenes [2000] and petroleum reservoir characterisation Mohaghegh et al. [1996]. Machine-learning methods, under which neural network approaches fall, are subdivided into classification and regression problems. Classification problems aim to divide data into subgroups, dependent on input multiple variables of input data. For example, a flower could be described by its colour, petal length, petal width, and number of petals. The combination of these features could identify the species a certain flower belongs to. By teaching the neural network which combinations of parameters belong to a certain species of flower, the neural network can start identifying species of flowers based on a combination of input parameters. Regression problems aim to provide a specific value for an output parameter on a continuous spectrum based on a combination of input parameters. A neural network could give the predicted value of a house based on, for example, its number of bedrooms, location, build year, and energy label. The output value is not a type A versus type B answer, but rather a point on a continuous value function. For regression problems such as the prediction of porosity and permeability of a reservoir rock, fuzzy logic, as opposed to Boolean logic, can be used. Fuzzy logic allows for a partial truth a value between 0 and 1 rather than a hard

1 or a 0 as used in Boolean logic. This results in the possibility to weigh the importance of a parameter in a process Zadeh [1976]. Lin (1994) introduces fuzzy curves to find a relationship between every input parameter and the output parameter. An important characteristic of fuzzy logic is that it allows the quantification of uncertainty. Still, since the modelling is data driven, the effort should be reviewed where multiple realizations of the geologic model are generated Ouenes [2000] General Regression Neural Networks can be used as a first step to finding the optimal network design Mohaghegh et al. [1996]. Backpropagation is a method for solving regression problems which allows for detection of non-linear relationships. The Neural Net identifies the optimal weight matrix for input parameters minimizing the quadratic error. A Multi-Layer Perceptron (MLP) can be used, which estimates an output (f(X)) from a set of input (x1, x2). Hidden layers perform non-linear transformations which allows the algorithm to find non-linear relationships between input and output. A visual representation is given in figure 2.

A.11 Conclusions

A study of microbial degradation in sedimentary systems with a common brine composition can thus be used in applications for sedimentary geothermal systems, geothermal resource from petroleum reservoirs, and CCS. show a lower permeability than fresh samples . Values for mineralogy, porosity, and permeability of Bentheimer Sandstone from previous studies are valuable as they provide a strong framework for realistic measurement values. Still, the research towards microbial reservoir degradation will need to determine exact values for all samples to determine the effects of metabolic treatment more accurately. When researching microbial degradation of sandstone, it is useful to provide context of well-known mechanism of sandstone corrosion. When prerequisites for sandstone corrosion are known, observed results from metabolic treatment might be explained. Laboratory Experiment In simulating an in-situ environment of a sedimentary low temperature geothermal field or a CCS reservoir, the following things are deduced from the literature review

1. Using a sandstone such as Bentheimer Sandstone is relevant to the settings that will be researched.

2. Temperatures in sedimentary geothermal systems usually do not exceed 150 C.

3. Conditions can be assumed to be anaerobic.

4. Brines usually contain salts and a mixture of rock forming elements in solution.

5. Pressure depends on the depth of the reservoir but sedimentary geothermal systems are commonly in the range of 2-5 km depth.

Pressure and temperature are important factors in the pathway of any dissolution and precipitation processes. Microbial corrosion of inorganic substrates is mainly done through excretion of organic solvents and organic acids. Furthermore, the formation of biofilm is stimulating factor for degradation. Examples of acids that can cause corrosion of inorganic substrates are acetic acid and butyric acid. Organic solvents can also act as chelating agents. Sandstone corrosion can happen through water-rock interactions in the presence of CO_2 without any microbial activity. Addition of metabolites could have an increased effect. Bentheimer Sandstone is a relatively pure sandstone (91.70 wt quartz). However, presence of feldspar and iron hydroxides gives rise to the hypothesis that these components could be involved in dissolution and precipitation processes during metabolic treatment. Moreover, at high temperatures and in an anaerobic environment, the solubility of Si is expected to increase. Measurements of porosity and permeability can be done using standard methodologies. Confined strength measurements can be done simultaneously with permeability measurements. However, since confined strength measurements will destroy samples, this can only be done after metabolic treatment has been done. Flow inversion during permeability measurements can yield insight into the extent of pore clogging by small solid particles in degraded rock. Overall, several mechanisms are expected to impact porosity and permeability of the Bentheimer Sandstone. Dissolution of the Sandstone can occur, potentially increasing porosity and permeability. Precipitation of new minerals could occur, reducing porosity and permeability. Small solid particles might cause pore clogging, reducing permeability. Structural integrity of the Sandstone could be reduced, potentially leading to fracturing of the sample, increasing porosity and permeability. Neural Networks can find relationships between input parameters and an output parameter in highly complex systems. Back-propagation is a commonly used method in solving regression problems with respect to reservoir parameters. Relative impact of geological input factors can be determined using fuzzy curves.

Appendix B

Raw Data of Experiments

Table B.1: Measured parameters of the initial state of samples

Initial state										
Sample	height (cm)	diameter (cm)	Vma(kN/m3)	Vb(kN/m3)	p dry (%)	p wet(%)	perm dry(D)	perm wet (D)	dry weight (g)	wet weight (g)
x1	3.480	2.950	17.535	23.785	0.263	0.252	2.020	1.250	47.200	29.420
x2	3.500	2.940	17.372	23.760	0.269	0.250	2.936	1.218	47.280	29.470
x3	3.450	2.950	17.345	23.580	0.264	0.246	2.568	1.271	46.700	28.930
x4	3.500	2.950	16.839	23.922	0.296	0.252	3.131	1.419	47.000	29.100
x5	3.520	2.950	17.461	24.058	0.274	0.243	2.500	1.258	47.830	29.620
x6	3.550	2.950	17.122	24.263	0.294	0.241	2.279	1.052	48.100	29.690
x7	3.520	2.930	17.687	23.733	0.255	0.229	2.486	1.721	47.900	29.600
x8	3.480	2.950	17.425	23.785	0.267	0.252	2.614	1.345	47.060	29.270
x9	3.500	2.950	17.310	23.922	0.276	0.253	3.084	1.361	47.260	29.380
x10	3.520	2.950	17.242	24.058	0.283	0.253	2.669	1.374	47.500	29.530
x11	3.330	2.950	16.683	22.760	0.267	0.254	3.139	1.304	44.980	27.990
x12	3.410	2.930	17.252	22.991	0.250	0.239	2.597	1.132	46.330	28.840
x13	3.380	2.950	16.957	23.101	0.266	0.254	2.886	1.284	45.600	28.370
x14	3.400	2.950	17.115	23.238	0.264	0.253	2.461	1.235	46.000	28.640
averages	3.467	2.946	17.239	23.640	0.271	0.248	2.669	1.302	46.910	29.132
y1	3.500	2.950	17.618	23.922	0.264	0.258	2.343	1.202	47.140	29.390
y2	3.500	2.950	17.397	23.922	0.273	0.248	2.821	1.467	47.410	29.410
y3	3.490	2.930	17.399	23.531	0.261	0.248	2.730	1.422	46.860	29.160
y4	3.450	2.950	17.188	23.580	0.271	0.254	2.545	1.493	46.590	29.010
y5	3.480	2.950	17.509	23.785	0.264	0.247	1.973	0.887	47.210	29.310
y6	3.420	2.950	17.297	23.375	0.260	0.243	2.289	1.020	46.650	28.950
y7	3.420	2.940	17.024	23.217	0.267	0.248	2.422	1.323	46.170	28.700
y8	3.410	2.950	17.121	23.306	0.265	0.252	2.562	1.640	46.160	28.720
y9	3.340	2.950	16.708	22.828	0.268	0.254	2.213	1.017	45.230	28.190
y10	3.380	2.950	16.891	23.101	0.269	0.256	2.239	1.416	45.600	28.420
y11	3.380	2.950	16.933	23.101	0.267	0.255	2.008	1.068	45.740	28.530
averages	3.434	2.947	17.189	23.424	0.266	0.251	2.377	1.269	46.433	28.890
z1	3.400	2.950	16.793	23.238	0.277	0.249	2.578	1.437	45.730	28.270
z2	3.350	2.950	16.851	22.896	0.264	0.265	2.563	1.771	45.210	28.380
z3	3.420	2.950	17.208	23.375	0.264	0.253	3.177	1.822	46.210	28.740
z4	3.350	2.950	17.121	22.896	0.252	0.251	2.631	1.688	45.380	28.220
z5	3.400	2.950	17.137	23.238	0.263	0.253	2.624	1.620	45.930	28.580
z6	3.400	2.950	17.117	23.238	0.263	0.251	2.856	1.616	46.040	28.630
z7	3.410	2.950	17.118	23.306	0.266	0.257	3.098	1.720	45.900	28.580
z8	3.410	2.950	17.225	23.306	0.261	0.250	3.540	1.851	46.210	28.740
z9	3.410	2.950	17.238	23.306	0.260	0.249	3.424	1.664	46.300	28.800
z10	3.420	2.950	17.238	23.375	0.263	0.244	3.480	1.664	46.620	28.950
z11	3.410	2.950	17.116	23.306	0.266	0.250	3.144	1.668	46.220	28.730
averages	3.398	2.950	17.106	23.226	0.263	0.252	3.010	1.684	45.977	28.601

TABLE B.2: Measured Parameters of the final state of samples

Final state Sample	height(cm)	diameter(cm)	Vma(kN/m3)	Vb(kN/m3)	p dry (%)	p wet(%)	perm dry(D)	perm wet (D)	dry weight (g)	wet weight (g)
x1	3.480	2.950	17.548	23.785	0.262	0.248	1.901	0.661	47.190	29.300
x2	3.500	2.940	17.597	23.760	0.259	0.248	2.647	1.014	47.280	29.410
x3	3.450	2.950	17.418	23.580	0.261	0.253	2.262	0.626	46.670	29.050
x4	3.500	2.950	17.534	23.922	0.267	0.260	2.606	0.889	46.930	29.220
x5	3.520	2.950	17.898	24.058	0.256	0.248	2.043	0.835	47.790	29.710
x6	3.550	2.950	17.961	24.263	0.260	0.251	2.037	0.720	48.050	29.880
x7	3.520	2.930	17.903	23.733	0.246	0.238	3.509	0.724	47.870	29.780
x8	3.480	2.950	17.564	23.785	0.262	0.251	2.448	0.688	47.080	29.270
x9	3.500	2.950	17.649	23.922	0.262	0.255	3.179	0.696	47.240	29.420
x10	3.520	2.950	17.791	24.058	0.261	0.255	2.717	0.843	47.500	29.570
x11	3.330	2.950	16.825	22.760	0.261	0.253	2.797	0.922	44.970	27.970
x12	3.410	2.930	17.342	22.991	0.246	0.238	2.479	0.770	46.330	28.820
x13	3.380	2.950	17.051	23.101	0.262	0.255	2.862	0.925	45.600	28.390
x14	3.400	2.950	17.236	23.238	0.258	0.253	2.160	0.614	45.990	28.630
averages	3.467	2.946	17.523	23.640	0.259	0.250	2.546	0.780	46.892	29.173
y1	3.500	2.950	17.684	23.922	0.261	0.249	2.701	0.710	47.180	29.210
y2	3.500	2.950	17.787	23.922	0.256	0.245	2.749	1.095	47.450	29.390
y3	3.490	2.930	17.847	23.531	0.242	0.222	2.682	1.022	47.510	29.210
y4	3.450	2.950	17.633	23.580	0.252	0.237	3.228	1.191	46.930	28.930
y5	3.480	2.950	17.841	23.785	0.250	0.235	2.805	0.646	47.470	29.270
y6	3.420	2.950	18.609	23.375	0.204	0.137	3.504	0.774	49.110	28.940
y7	3.420	2.940	17.303	23.217	0.255	0.245	3.528	1.424	46.170	28.630
y8	3.410	2.950	17.254	23.306	0.260	0.250	3.214	1.041	46.110	28.630
y9	3.340	2.950	16.910	22.828	0.259	0.249	2.692	0.864	45.210	28.070
y10	3.380	2.950	17.041	23.101	0.262	0.255	3.463	0.600	45.610	28.410
y11	3.380	2.950	17.140	23.101	0.258	0.249	2.355	0.758	45.740	28.400
averages	3.434	2.947	17.550	23.424	0.251	0.234	2.993	0.920	3.993	28.826
z1	3.400	2.950	17.145	23.238	0.262	0.256	2.113	0.238	45.730	28.430
z2	3.350	2.950	16.961	22.896	0.259	0.251	2.540	0.916	45.210	28.060
z3	3.420	2.950	17.339	23.375	0.258	0.250	3.527	1.177	46.210	28.670
z4	3.350	2.950	16.986	22.896	0.258	0.275	2.379	1.205	45.280	28.670
z5	3.400	2.950	17.259	23.238	0.257	0.250	2.601	1.011	45.950	28.520
z6	3.400	2.950	17.292	23.238	0.256	0.248	3.088	1.108	46.050	28.570
z7	3.410	2.950	17.238	23.306	0.260	0.247	3.493	1.416	45.880	28.340
z8	3.410	2.950	17.338	23.306	0.256	0.244	3.214	1.202	46.180	28.570
z9	3.410	2.950	17.372	23.306	0.255	0.247	3.051	1.264	46.270	28.720
z10	3.420	2.950	17.470	23.375	0.253	0.241	2.966	1.125	46.550	28.810
z11	3.410	2.950	17.686	23.306	0.241	0.217	1.258	1.121	46.920	28.660
averages	2.748	2.748	2.748	2.748	2.748	2.748	2.748	1.071	46.021	28.547

Table B.3: Weight evolution of samples (g)

(g)	Start		Alginate		Filters	Final		differential	
	dry weight	wet weight	without	with	mass removed	dry weight	wet weight		
x1	47.2	29.42	46.67	49.03	0.0002	47.19	29.3	-0.01	-0.12
x2	47.28	29.47	46.82	49.37	0.0073	47.28	29.41	0	-0.06
x3	46.7	28.93	46.1	47.81	0.3362	46.67	29.05	-0.03	0.12
x4	47	29.1	46.9185	49.4306	0.357	46.93	29.22	-0.07	0.12
x5	47.83	29.62	47.7768	50.6567	0.6053	47.79	29.71	-0.04	0.09
x6	48.1	29.69	48.0466	50.528	0.4305	48.05	29.88	-0.05	0.19
x7	47.9	29.6	46.73	49.24	0.0859	47.87	29.78	-0.03	0.18
x8	47.06	29.27	46.68	48.74	0.1828	47.08	29.27	0.02	0
x9	47.26	29.38	46.81	49.44	0.0767	47.24	29.42	-0.02	0.04
x10	47.5	29.53	47.4567	49.9449	0.7872	47.5	29.57	0	0.04
x11	44.98	27.99	44.934	47.0914	0.567	44.97	27.97	-0.01	-0.02
x12	46.33	28.84	46.2894	48.4589	0.6862	46.33	28.82	0	-0.02
x13	45.6	28.37	45.11	46.94	0.1791	45.6	28.39	0	0.02
x14	46	28.64	45.47	48.16	0.4892	45.99	28.63	-0.01	-0.01
y1	47.14	29.39	46.66	49.14	0.2224	47.18	29.21	0.04	-0.18
y2	47.41	29.41	47.1	49.69	0.151	47.45	29.39	0.04	-0.02
y3	46.86	29.16	46.48	48.57	0.2957	47.51	29.21	0.65	0.05
y4	46.59	29.01	46.6129	49.0874	0.5176	46.93	28.93	0.34	-0.08
y5	47.21	29.31	47.1629	49.2602	0.942	47.47	29.27	0.26	-0.04
y6	46.65	28.95	46.1367	48.9132		49.11	28.94	2.46	-0.01
y7	46.17	28.7	45.78	47.97	0.2535	46.17	28.63	0	-0.07
y8	46.16	28.72	45.84	47.41	0.3196	46.11	28.63	-0.05	-0.09
y9	45.23	28.19	44.82	46.67	0.2371	45.21	28.07	-0.02	-0.12
y10	45.6	28.42	45.33	47.31	0.1628	45.61	28.41	0.01	-0.01
y11	45.74	28.53	45.29	47.81	0.1518	45.74	28.4	0	-0.13
z1	45.73	28.27	45.7066	47.2341	0.3334	45.73	28.43	0	0.16
z2	45.21	28.38	45.1712	47.4079		45.21	28.06	0	-0.32
z3	46.21	28.74	46.1884	48.5346	0.5534	46.21	28.67	0	-0.07
z4	45.38	28.22	45.2858	47.7656	0.4274	45.28	28.67	-0.1	0.45
z5	45.93	28.58	45.9343	48.4045	0.7519	45.95	28.52	0.02	-0.06
z6	46.04	28.63	46.0441	48.4035	0.4021	46.05	28.57	0.01	-0.06
z7	45.9	28.58	45.8548	48.0296	0.3956	45.88	28.34	-0.02	-0.24
z8	46.21	28.74	46.1601	48.4463	0.5866	46.18	28.57	-0.03	-0.17
z9	46.3	28.8	46.2475	48.356	0.5579	46.27	28.72	-0.03	-0.08
z10	46.62	28.95	46.9185	49.6322	0.4118	46.55	28.81	-0.07	-0.14
z11	46.22	28.73	46.1367	48.6407		46.92	28.66	0.7	-0.07

TABLE B.4: average values and standard deviation for porosity and permeability values

Initial	average p dry (%)	stand. dev. p dry (%)	average perm dry (D)	stand. dev. perm dry (D)
x	0.270615353	0.010183603	2.669314091	0.2612604
y	0.266177117	0.003183197	2.376778338	0.217456994
z	0.263494399	0.003438369	3.010324266	0.327303765
	average p wet (%)	stand dev p wet (%)	average perm wet (D)	stand. dev. perm wet (D)
x	0.24798524	0.005857355	1.301731347	0.101940781
y	0.251098795	0.004080874	1.268676122	0.209001287
z	0.25190471	0.003668893	1.683681723	0.078825586
	unit density kg/m3	unit weight kN/m3		
x	1.984374725	19.46671605		
y	1.982247963	19.44585252		
z	1.979591087	19.41978856		
Final				
	average p dry (%)	stand. dev. p dry (%)	average perm dry (D)	stand. dev. perm dry (D)
x	0.258738941	0.004174299	2.546288285	0.35628064
y	0.250798197	0.010373032	2.992642863	0.358677912
z	0.255985326	0.003580094	2.748259992	0.51829559
	average p wet (%)	stand dev p wet (%)	average perm wet (D)	stand. dev. perm wet (D)
x	0.25042694	0.004533227	0.780484373	0.106488494
y	0.233925806	0.019718238	0.920377794	0.212773192
z	0.247709838	0.007662294	1.071025137	0.190626145
	unit density kg/m3	unit weight kN/m3		
x	1.983619337	19.45930569		
y	1.996724009	19.58786252		
z	1.981469888	19.4382196		
Difference				
	average p dry (%)	stand. dev. p dry (%)	average perm dry (D)	stand. dev. perm dry (D)
x	-0.011876411	-0.006009304	-0.123025806	0.09502024
y	-0.01537892	0.007189834	0.615864525	0.141220918
z	-0.007509073	0.000141725	-0.262064274	0.190991825
	average p wet (%)	stand dev p wet (%)	average perm wet (D)	stand. dev. perm wet (D)
x	0.002441701	-0.001324128	-0.521246974	0.004547713
y	-0.017172989	0.015637365	-0.348298329	0.003771905
z	-0.004194872	0.003993401	-0.612656586	0.111800559
	unit density kg/m3	unit weight kN/m3		
x	-0.000755388	-0.007410359		
y	0.014476045	0.142010004		
z	0.001878801	0.01843104		

Table B.5: MLP Weights

Prediction Dry Permeability Weights MLP								
	1	2	3	4				
Inipor (d)	-1.5758771	13.68531313	-4.71129414	4.14363709				
					1	2	3	4
iniperm (d)	-1.62262191	-1.35179303	-0.32608128	-1.55631972	-1.60158325	-18.08780466	-0.99738524	4.50131366
T	-4.15699804	-1.14195383	-7.63814217	0.09611561				
Conc	0.77951309	-0.08936737	0.38342128	-0.80779303				
Prediction Dry Porosity Weights MLP								
	1	2	3	4				
Inipor (d)	0.05139716	-0.25497881	0.39516834	0.01679287				
					1	2	3	4
iniperm (d)	0.48530877	-0.63671444	-0.69144894	-0.699608	-0.21308388	-0.426071	-0.39454231	0.26602754
T	-0.46020654	0.79784594	-0.21827237	0.19891156				
Conc	-0.1800343	0.08291532	0.42577219	0.8106171				
Prediction Wet Permeability Weights MLP								
	1	2	3	4				
Inipor (w)	3.58639228	-0.32868718	-14.1325258	-0.02617946				
					1	2	3	4
Iniperm (w)	0.65680696	0.03664678	2.24171172	-0.93937185	-4.06228931	1.35519793	7.41816797	-2.33055909
T	-0.88869231	-0.83491747	1.36123224	-3.73781035				
Conc	0.31363677	-0.32566307	0.53532192	-0.01499716				
Prediction Wet Porosity Weights MLP								
	1	2	3	4				
Inipor (w)	0.84952272	0.5106257	0.43230656	-0.42276459				
					1	2	3	4
iniperm (w)	0.30247271	0.48150729	0.50199555	0.50406373	-0.66296871	0.35873405	0.24723053	0.5107586
T	0.71935455	0.73278545	0.25534497	-0.27215202				
Conc	0.14463894	0.25916864	0.17762301	0.01911778				

Appendix C

Neural Network Scripts

```
#!/usr/bin/env python
# coding: utf-8

# In[1]:


#####  import needed modules ########
import numpy as np
import pandas as pd
import seaborn as sns
import sklearn as skl
import matplotlib.pyplot as plt
get_ipython().run_line_magic('matplotlib', 'inline')

#####  read data #######

data1 = pd.read_excel("C:/Users/Arjen/Documents/Msc Thesis/ML excel files/boston36smpls.xlsx")
data2 = pd.read_excel("C:/Users/Arjen/Documents/Msc Thesis/ML excel files/boston70smpls.xlsx")
data3 = pd.read_excel("C:/Users/Arjen/Documents/Msc Thesis/ML excel files/boston150smpls.xlsx")
data4 = pd.read_excel("C:/Users/Arjen/Documents/Msc Thesis/ML excel files/boston500smpls.xlsx")


# In[2]:


#######  select input and target data for all data sets ######
X1 = data1[['INDUS', 'NOX', 'RM', 'TAX']]
y1 = data1[['MV']]

X2 = data2[['INDUS', 'NOX', 'RM', 'TAX']]
y2 = data2[['MV']]
```

```
X3 = data3[['INDUS', 'NOX', 'RM', 'TAX']]
y3 = data3[['MV']]

X4 = data4[['INDUS', 'NOX', 'RM', 'TAX']]
y4 = data4[['MV']]

################  normalise data ##########################

from sklearn import preprocessing
X1 = preprocessing.normalize(X1)
X2 = preprocessing.normalize(X2)
X3 = preprocessing.normalize(X3)
X4 = preprocessing.normalize(X4)

###############  train test split ########################

from sklearn.cross_validation import train_test_split
X_train, X_test, y_train, y_test = train_test_split(X1, y1)
X2_train, X2_test, y2_train, y2_test = train_test_split(X2, y2)
X3_train, X3_test, y3_train, y3_test = train_test_split(X3, y3)
X4_train, X4_test, y4_train, y4_test = train_test_split(X4, y4)


########## import models ###########
from sklearn.linear_model import LinearRegression
from sklearn.neural_network import MLPRegressor


######## instantiate models ############
linreg = LinearRegression()
mlpreg = MLPRegressor(activation='tanh', hidden_layer_sizes=4, learning_rate='adaptive', solver=



######### fit the model to the training data #############

##### Uncomment this section to use a least squares linear regression model #####

#linreg.fit(X_train, y_train)
#linreg.fit(X2_train, y2_train)
#linreg.fit(X3_train, y3_train)
#linreg.fit(X4_train, y4_train)

#############################################################################



### Uncomment this section to use a multi-layer perceptron ###
```

```
#mlpreg.fit(X_train, y_train)
#mlpreg.fit(X2_train, y2_train)
#mlpreg.fit(X3_train, y3_train)
#mlpreg.fit(X4_train, y4_train)

################################################################


# In[3]:


######## predict values #############

#y_pred = linreg.predict(X_test)
#y2_pred = linreg.predict(X2_test)
#y3_pred = linreg.predict(X3_test)

#y_pred = mlpreg.predict(X_test)
#y2_pred = mlpreg.predict(X2_test)
#y3_pred = mlpreg.predict(X3_test)
#y4_pred = mlpreg.predict(X4_test)

#print np.shape(y4_pred)
#print y_pred
#print y_pred2
#print y_test


# In[4]:


### create x-arrays for plotting ####
x = np.array(range(1,10))
x2 = np.array(range(1,19))
x3 = np.array(range(1,39))
x4 = np.array(range(1,126))


# In[5]:


#### Plot 36 sample predictions #####

plt.plot(x, y_pred, 'go')
plt.plot(x, y_test, 'yo')
plt.xlabel('sample')
plt.ylabel('mean value ($ 10.000)')
```

```
# In[6]:


###### plot 70 sample predictions ########

plt.plot(x2, y2_pred, 'go')
plt.plot(x2, y2_test, 'yo')


# In[7]:


###### plot 150 sample predictions ########

plt.plot(x3, y3_pred, 'go')
plt.plot(x3, y3_test, 'yo')


# In[8]:


###### plot 500 sample predictions ########

plt.plot(x4, y4_pred, 'go')
plt.plot(x4, y4_test, 'yo')


# In[9]:


###### validate performance ######

### Uncomment this section to validate the linear model ###

#print linreg.score(X1, y1)
#print linreg.score(X2, y2)
#print linreg.score(X3, y3)
#print linreg.score(X3, y3)


### Uncomment this section to validat the multi-layer perceptron ###

print mlpreg.score(X1, y1)
```

```
print mlpreg.score(X2, y2)
print mlpreg.score(X3, y3)
print mlpreg.score(X4, y4)
```

```
#!/usr/bin/env python
# coding: utf-8

# In[3]:


#####  import needed modules ########

import numpy as np
import pandas as pd
import seaborn as sns
import sklearn as skl
import matplotlib.pyplot as plt


get_ipython().run_line_magic('matplotlib', 'inline')

#####  read data #######
data = pd.read_excel("C:/Users/Arjen/Documents/Msc Thesis/ML excel files/ML_DATA.xlsx")


# In[4]:


#######  select input and target data for the data set ######

X1 = data[['IniPor(w)', 'IniPerm(w)', 'Temp', 'Conc']]
y1 = data[['FinPor(w)']]
y2= data[['FinPerm(w)']]

################  normalise data ##########################

from sklearn import preprocessing
X1 = preprocessing.normalize(X1)



#from sklearn.model_selection import KFold
#kf = KFold(n_splits=3)

#for train_index, test_index in kf.split(X1):
    #print("TRAIN:", train_index, "TEST:", test_index)
    #X_train, X_test = X1[train_index], X1[test_index]
    #y_train, y_test = y1[train_index], y1[test_index]
```

```
# In[5]:


###############  train test split ########################

from sklearn.cross_validation import train_test_split
X_train, X_test, y_train, y_test = train_test_split(X1, y1, random_state=2)
X_train2, X_test2, y_train2, y_test2 = train_test_split(X1, y2, random_state=3)

########## import models ############
from sklearn.linear_model import LinearRegression
from sklearn.neural_network import MLPRegressor


######## instantiate models ############
linreg = LinearRegression()
mlpreg = MLPRegressor(activation='tanh',hidden_layer_sizes=4,learning_rate='adaptive', learning_

######### fit the model to the training data #############


##### Uncomment this section to use a least squares linear regression model #####
#linreg.fit(X_train, y_train)
#linreg.fit(X_train2, y_train2)

#################################################################################

### Uncomment this section to use a multi-layer perceptron ###

#mlpreg.fit(X_train, y_train)
mlpreg.fit(X_train2, y_train2)

#################################################################


# In[6]:


######## predict values #############

### linear regression ###
#y_pred = linreg.predict(X_test)
#y_pred2 = linreg.predict(X_test2)

### Multi-layer perceptron
```

```
#y_pred = mlpreg.predict(X_test)  #Porosity
y_pred2 = mlpreg.predict(X_test2) #Permeability


# In[7]:


### Get parameters ###

params =mlpreg.get_params()
print params

### create x-array for plotting ####
x = np.array(range(1,10))


# In[ ]:


plt.plot(x, y_pred, 'ro', label= 'predicted')
plt.plot(x, y_test, 'bo', label= 'real')
plt.title('MLPREG: Wet porosity prediction and real value compared')
plt.xlabel('Sample')
plt.ylabel('Porosity (%)')
plt.legend()


# In[8]:


x = np.array(range(1,10))

plt.plot(x,y_pred2, 'ro', label='predicted')
plt.plot(x,y_test2, 'bo', label='real')
plt.title('MLPREG:  Wet Permeability prediction and real value compared')
plt.xlabel('Sample')
plt.ylabel('Permeability (D)')
plt.legend()


# In[10]:


### Uncomment this section to validate the least squares linear regression model ###

#print linreg.score(X1,y1)
#print linreg.score(X1,y2)
```

```
### Uncomment this section to validate the Multi-layer Perceptron ###

#print mlpreg.score(X1,y1)
#print mlpreg.score(X1,y2)


# In[ ]:


y_pred = np.reshape(9,1)
y_pred2 = np.reshape(9,1)
linreg_error = np.subtract(y_pred, y_test)
linreg_error2 = np.subtract(y_pred2, y_test2)
linreg_rsme = np.sqrt((np.sum(linreg_error**2)/len(y_pred)))
linreg_rsme2 = np.sqrt((np.sum(linreg_error2**2)/len(y_pred2)))

print linreg_rsme, linreg_rsme2
```

Bibliography

A Barbacki. The use of abandoned oil and gas wells in poland for recovering geothermal heat. In *Proceedings World Geothermal Congress*, pages 3361–3365, 2000.

PC Bennett, JR Rogers, WJ Choi, and FK Hiebert. Silicates, silicate weathering, and microbial ecology. *Geomicrobiology Journal*, 18(1):3–19, 2001.

Pieter Bertier, Rudy Swennen, B Laenen, D Lagrou, and R Dreesen. Experimental identification of co2–water–rock interactions caused by sequestration of co2 in westphalian and buntsandstein sandstones of the campine basin (ne-belgium). *Journal of Geochemical Exploration*, 89(1-3):10–14, 2006.

Gunnar Bövarsson. *Utilization of geothermal energy for heating purposes and combined schemes involving power generation, heating and/or by-products.* 1964.

TP Clement, BM Peyton, RS Skeen, DA Jennings, and JN Petersen. Microbial growth and transport in porous media under denitrification conditions: experiments and simulations. *Journal of Contaminant Hydrology*, 24(3-4):269–285, 1997.

M Yavuz Corapcioglu and A Haridas. Microbial transport in soils and groundwater: A numerical model. *Advances in Water Resources*, 8(4):188–200, 1985.

Howard B Demuth, Mark H Beale, Orlando De Jess, and Martin T Hagan. *Neural network design*. Martin Hagan, 2014.

C Wim Dubelaar and Timo G Nijland. The bentheim sandstone: geology, petrophysics, varieties and its use as dimension stone. In *Engineering Geology for Society and Territory-Volume 8*, pages 557–563. Springer, 2015.

Thomas W Engler. Fluid flow in porous media. *Petroleum Engineering*, 524:2–1, 2010.

Sebastian Fischer, Kornelia Zemke, Axel Liebscher, Maren Wandrey, CO2SINK Group, et al. Petrophysical and petrochemical effects of long-term co2-exposure experiments on brine-saturated reservoir sandstone. *Energy Procedia*, 4:4487–4494, 2011.

Einar Gunnlaugsson, Halldór Ármannsson, Sverrir órhallsson, Benedikt Steingrímsson, et al. Problems in geothermal operation-scaling and corrosion. 2014.

Roland F Krueger et al. An overview of formation damage and well productivity in oilfield operations: An update. 1988.

Antonio C Lasaga. *Kinetics of geochemical processes*, volume 8. Mineralogical Society of Amer, 1981.

Dong C Liu and Jorge Nocedal. On the limited memory bfgs method for large scale optimization. *Mathematical programming*, 45(1-3):503–528, 1989.

Xiaolei Liu, Gioia Falcone, and Claudio Alimonti. A systematic study of harnessing low-temperature geothermal energy from oil and gas reservoirs. *Energy*, 142:346–355, 2018.

Michel Magot, Bernard Ollivier, and Bharat KC Patel. Microbiology of petroleum reservoirs. *Antonie van Leeuwenhoek*, 77(2):103–116, 2000.

Shahab Mohaghegh, Reza Arefi, Sam Ameri, Khashayar Aminiand, and Roy Nutter. Petroleum reservoir characterization with the aid of artificial neural networks. *Journal of Petroleum Science and Engineering*, 16(4):263–274, 1996.

Ellyn M Murphy and Timothy R Ginn. Modeling microbial processes in porous media. *Hydrogeology Journal*, 8(1):142–158, 2000.

Ahmed Ouenes. Practical application of fuzzy logic and neural networks to fractured reservoir characterization. *Computers & Geosciences*, 26(8):953–962, 2000.

Anna E Peksa, Karl-Heinz AA Wolf, and Pacelli LJ Zitha. Bentheimer sandstone revisited for experimental purposes. *Marine and Petroleum Geology*, 67:701–719, 2015.

MG Reed et al. Gravel pack and formation sandstone dissolution during steam injection. *Journal of Petroleum Technology*, 32(06):941–949, 1980.

Kristján Saemundsson et al. Geothermal systems in global perspective. 2013.

Wolfgang Sand. Microbial mechanisms of deterioration of inorganic substratesa general mechanistic overview. *International Biodeterioration & Biodegradation*, 40(2-4):183–190, 1997.

Wolfgang Sand. Microbial life in geothermal waters. *Geothermics*, 32(4-6):655–667, 2003.

Ryoji Shiraki and Thomas L Dunn. Experimental study on water–rock interactions during co2 flooding in the tensleep formation, wyoming, usa. *Applied Geochemistry*, 15(3):265–279, 2000.

Harkaran Singh, Gioia Falcone, Alexandre Volle, and Laurent Guillon. Harnessing geothermal energy from mature onshore oil fields-the wytch farm case study. 2017.

Nathalie Tufenkji. Modeling microbial transport in porous media: Traditional approaches and recent developments. *Advances in water resources*, 30(6-7):1455–1469, 2007.

Pierre Ungemach. Reinjection of cooled geothermal brines into sandstone reservoirs. *Geothermics*, 32(4-6):743–761, 2003.

AK Wojtanowicz, Z Krilov, and JP Langlinais. Experimental determination of formation damage pore blocking mechanisms. *Journal of energy resources technology*, 110(1): 34–42, 1988.

Lotfi A Zadeh. A fuzzy-algorithmic approach to the definition of complex or imprecise concepts. In *Systems Theory in the Social Sciences*, pages 202–282. Springer, 1976.